# Title: Neutrophil extracellular traps drive inflammatory pathogenesis in malaria


**Authors:**

Sebastian Lorenz Knackstedt[1], Athina Georgiadou[2], Falko Apel[1], Ulrike Abu-Abed[3], Christopher A. Moxon[4], Aubrey J. Cunnington[2], Bärbel Raupach[1], Deirdre Cunningham[5], Jean Langhorne[5], Renate Krüger[6], Valentina Barrera[7], Simon P. Harding[7], Aase Berg[8], Sam Patel[9], Kari Otterdal[10], Benjamin Mordmüller[11,12],Evelin Schwarzer[13], Volker Brinkmann[3], Arturo Zychlinsky[1] and Borko Amulic[1,14*]

**Affiliations:**

[1] Max Planck Institute for Infection Biology, Department of Cellular Microbiology, Charitéplatz 1, 10117 Berlin, Germany
[2]Section of Paediatrics, Imperial College London
[3] Max Planck Institute for Infection Biology, Microscopy Core Facility, Charitéplatz 1, 10117 Berlin, Germany
[4] Wellcome Centre for Integrative Parasitology, Institute of Infection Immunity and Inflammation, University of Glasgow
[5] The Francis Crick Institute, 1 Midland Road, London NW1 1AT, UK
[6] Charité - Universitätsmedizin Berlin, Humboldt-Universität zu Berlin and Berlin Institute of Health, Department of Pediatric Pneumology, Immunology and Intensive Care, Berlin, Germany
[7] Department of Eye and Vision Science, Institute of Ageing and Chronic Disease, University of Liverpool, a member of Liverpool Health Partners
[8] Stavanger University Hospital, Stavanger, Norway
[9] Maputo Central Hospital, Maputo, Mozambique
[10] Research Institute of Internal Medicine, Oslo University Hospital Rikshospitalet, Oslo, Norway
[11] Centre de Recherches Médicales de Lambaréné (CERMEL), Lambaréné, Gabon.
[12] Universität Tübingen, Institut für Tropenmedizin, Wilhelmstraße 27, 72074 Tübingen
[13] Department of Oncology, University of Turin, Via Santena 5bis, 10126 Turin, Italy
[14] University of Bristol, School of Cellular and Molecular Medicine, Bristol, BS8 1TD, UK
* Correspondence and materials requests: borko.amulic@bristol.ac.uk

**One Sentence Summary:** We show that NETs contribute to the pathogenesis of malaria by promoting emergency granulopoiesis and facilitating cytoadhesion of parasitized erythrocytes to the endothelium.


## Abstract

Neutrophils are essential innate immune cells that extrude chromatin in the form of neutrophil extracellular traps (NETs). This form of cell death has potent immunostimulatory activity. We show that heme-induced NETs are essential for malaria pathogenesis. Using patient samples and a mouse model, we define two mechanisms of NET-mediated inflammation of the vasculature: activation of emergency granulopoiesis via GCSF production, and induction of the endothelial cytoadhesion receptor ICAM-1. Soluble NET components facilitate parasite sequestration and mediate tissue destruction. We demonstrate that neutrophils have a key role in malaria immunopathology and propose inhibition of NETs as a treatment strategy in vascular infections.

## Introduction

Neutrophils are the most abundant leukocytes in the blood and they respond to pathogens by phagocytosis, generation of oxidants and externalization of microbicidal peptides and proteases [1]. The release of these compartmentalized antimicrobials is achieved by either degranulation or the release of neutrophil extracellular traps (NETs). NETs consist of decondensed chromatin decorated with microbicidal and immunostimulatory molecules [2, 3]. NETs are released by a cell death program termed 'NETosis' and they ensure high local concentrations of active antimicrobials. Eventually, deoxyribonuclease 1 (DNase 1), a constitutive plasma endonuclease, degrades NETs and facilitates their removal [4].

NETosis is an active process that requires microbial or mitogenic signaling [5, 6], the production of reactive oxygen species (ROS) [7], the activity of two serine proteases: neutrophil elastase (NE) and proteinase 3 (PR3) [8, 9], and the activation of the pore forming protein gasdermin D [10]. NE translocates from the granules to the nucleus during NET induction, where it cleaves histones to allow chromatin decondensation prior to plasma membrane breakdown [8]. NE and PR3 have partially overlapping substrates [11] and are both required for maximal NET induction *in vivo* [9].

Triggering of NETosis by various microbes in tissues or the mucosa limits pathogen proliferation and dissemination [12]. NET release inside the vasculature, however, can be pathogenic by triggering autoimmunity [13], as well as by directly damaging blood vessels [14, 15] and inducing thrombosis [16].

To understand the role of neutrophils and NETs in intravascular infections, we investigated malaria, a disease caused by protozoan parasites that invade red blood cells (RBCs) and trigger systemic neutrophil activation [17, 18]. *Plasmodium*

*falciparum* is the most important and virulent species, causing over 200 million malaria episodes and close to 500,000 deaths annually [19]. It encompasses diverse pathological manifestations that can range from mild unspecific symptoms, fever and mild anemia to organ failure, acidosis, coma and death. Complications of severe malaria include coma, prostration, respiratory distress, metabolic acidosis, renal failure, liver damage and severe anemia [20, 21].

Pathogenesis of *P. falciparum* malaria is precipitated by its interaction with the vascular endothelium. In the second half of the asexual erythrocytic lifecycle, parasites express cytoadhesion factors on the surface of infected RBCs (iRBCs), allowing binding and sequestration in postcapillary venules. Attachment and withdrawal from circulation is thought to aid in preventing clearance of iRBCs by splenic macrophages [22]. Disease severity is synergistically determined by sequestration patterns and host inflammatory responses [23, 24]. Cytoadhesion of iRBCs leads to endothelial activation and vascular occlusion [24], while release of pathogen- or danger-associated molecular pattern (PAMP or DAMP) molecules leads to pathological inflammatory responses mediated by cytokines such as tumor necrosis factor (TNF) and interleukin (IL)-1β [25]. Organ-specific iRBC sequestration is associated with corresponding pathology [23, 24].

Despite the important inflammatory component of the disease, the role of neutrophils in *P. falciparum* malaria remains unclear. Neutrophils isolated from malaria patients have a reduced capacity to mount an oxidative burst [26]. On the other hand, several studies have linked activation of these cells to pathogenesis and severe disease [17, 18, 27]. For instance, a recent blood transcriptomic analysis comparing severe and uncomplicated malaria identified a granulocyte colony stimulating factor (GCSF)-regulated neutrophil granulopoiesis signature as a specific feature of severe malaria [18] . Granulopoiesis refers to production of neutrophils from progenitor cells

in the bone marrow; this blood signature therefore identifies increased neutrophil abundance as a pathogenic factor in malaria. Furthermore, genes encoding neutrophil granule proteins, such as NE and matrix metalloproteinase-8 (MMP-8), showed the highest upregulation between severe and uncomplicated malaria [18]. Similarly, a study in Malawi demonstrated that retinopathy-positive cerebral malaria is specifically associated with accumulation of externalized neutrophil proteins such as NE and PR3 [17]. Several studies in mice have also linked neutrophils to severe malaria [28-31]. Notably, depletion of neutrophils with a specific antibody reduces pathology in *Plasmodium chabaudi chabaudi* mouse infections [28].

In addition to the accumulation of soluble neutrophil proteases, severe disease is associated with an increase in extracellular human nucleosomes in patients' plasma [32], which could indicate NET release. NETs are a platform for externalizing both nucleosomes and neutrophil proteases and could thus be an important pathogenic factor in malaria. Indeed, NETs were reported in mouse malaria [31] and NET-like structures were observed on patient blood smears [33, 34].

We show, using patient samples, that NETs are triggered by extracellular heme in malaria. We found NETs to be a source of immunostimulatory molecules - alarmins - that activate emergency hematopoiesis via GCSF induction. In the *P. chabaudi* mouse model, host DNase 1 liberated neutrophil proteins from NETs and this release was required for neutrophilia and neutrophil infiltration in the liver. Soluble NET components were also required for parasite sequestration in liver and lung. Genetic depletion of NETs, or NET-processing DNase 1, reduced organ damage. We demonstrate an undescribed physiological role for NETs in circulation, as well as identify a potential target for adjunctive malaria therapy.

## Results

### Intravascular NET formation in *P. falciparum* malaria

To test if *P. falciparum* malaria is accompanied by *bona fide* NET induction, we initially analyzed plasma samples from forty-three parasitologically confirmed pediatric and adult patients, treated at the Albert Schweitzer Hospital, in Lambaréné, Gabon, a highly malaria-endemic region in Central Africa. The patients presented with variable symptoms such as hyperparasitemia, fever and anemia (Table S1) but did not show severe symptoms, and all recovered upon antimalarial treatment. NETs are defined as complexes of chromatin and neutrophil granule proteins; hence, we used an ELISA that detects NETs with an anti-DNA detection antibody, preceded by a capture antibody against NE. Malaria patients had significantly elevated levels of NETs compared to healthy controls from the same region (n = 9) (Fig. 1A).

To test if NETs are linked to malaria severity we next measured NE-DNA complexes in plasma from two different patient cohorts, each consisting of uncomplicated and severe malaria. The first cohort again consisted of pediatric patients from Lambaréné, Gabon, recruited in 1995 and 1996 as part of a case-control study with a subsequent longitudinal survey comparing severe (n=23) with strictly defined uncomplicated malaria cases (n=10; Table S2). Most children had severe anemia or hyperparasitemia and other complications; mortality was 3% [35]. The second cohort were 28 uncomplicated and 27 severe malaria HIV-negative adult in-patients at Central Hospital in Maputo, Mozambique. Severe malaria in this cohort was defined according to the severity criteria developed by the World Health Organization [36] and included cerebral malaria (CM), respiratory distress, liver failure and severe anemia (Table S2). In both cohorts NETs were significantly enriched in severe versus uncomplicated malaria (Fig. 1B and C).

We also isolated peripheral blood neutrophils from hospitalized adult patients and monitored NET formation. Neutrophils from malaria patients (n = 8) released twofold more NETs than healthy controls (n = 6) (Fig. 1D). Importantly, NETs were released without the addition of exogenous stimuli, indicating that NETosis in malaria is activated *in vivo*.

To further demonstrate NETs *in vivo* and to examine their association with neurovascular sequestration of infected red blood cells (iRBCs), a key event in CM pathogenesis, we examined retinal tissue from fatal paediatric cases who had died with a clinical diagnosis of cerebral malaria. Retinopathy is a highly specific feature of CM [37], and pathological changes in the retinal vasculature in CM are representative of those in the cerebral microvasculature [38, 39]. Through post mortem examination, cases were divided into those who had sequestration of parasitized erythrocytes in the brain and no alternative cause of death and were deemed to have 'true' CM, and those who had no sequestration and were in fact all found to have alternative causes of death. This second "faux CM" group is a useful comparator group to control for the effect of fatal encephalopathy and premorbid events versus those that are due to parasite sequestration. We analysed the retinas of nine definitive CM cases and eight comatose malaria cases without retinopathy (Table S3) and identified NETs by co-localization of citrullinated histone H3, elastase and DAPI. As expected, most of the retinal capillaries in true CM cases were packed with sequestered parasitized RBCs (Fig 1E). NETosis was detected exclusively in retinopathy positive CM cases (9/9) and localized only to areas with parasitized RBCs (Fig. 1F and G). Z-stack imaging revealed that NETs filled the lumen of retinal capillaries (Fig. 1G), enveloping the parasitized erythrocytes. Together, these data demonstrate that NETs are induced in the vasculature of malaria patients and that this correlates with parasite sequestration and disease severity.

192

193 **NETs in malaria are induced by heme and TNF**

194 To identify factors that trigger NET formation in malaria, we co-incubated neutrophils
195 from healthy adult donors with *P. falciparum* cultures. Neutrophils were either primed
196 with TNF, a major malaria-associated proinflammatory cytokine [24], or left unprimed.
197 We exposed neutrophils to iRBCs, free merozoites, parasite digestive vacuoles, which
198 are released upon RBC rupture and contain the hemozoin crystal, as well as heme, a
199 known malaria DAMP that is released during parasite egress, as well as during
200 'bystander hemolysis' – the inflammatory destruction of uninfected RBCs [25, 26].
201 Interestingly, only heme robustly induced NETs in combination with TNF priming (Fig.
202 2A & S1A), as previously reported in sickle cell disease [40].

203 To verify that NET formation is linked to hemolysis *in vivo*, we determined the
204 plasma free heme concentrations in our patient cohorts and examined their
205 association with plasma NE-DNA complexes. We found that free heme positively
206 correlates with circulating NETs in both Gabon cohorts (Fig. 2B and C) but not in the
207 adult Mozambique patients (Fig. 2D), possibly due to some very high heme values in
208 the latter. Consequently, we incubated neutrophils from healthy donors with plasma
209 from patients to test if soluble factors are sufficient to induce NETs. Plasma from
210 severe, but not mild malaria was sufficient to induce NETs in healthy neutrophils and
211 this effect was abolished by the heme scavenger hemopexin (Fig. 2E). In summary,
212 accumulation of free heme during malaria activates neutrophils to release NETs.

213

214 **Heme-induced NETs require oxidants and NE/PR3 mediated proteolysis**

215 There are different pathways leading to NET formation [41]. We tested the
216 involvement of host factors previously implicated in NETosis, starting with the ROS-
217 producing enzyme NOX2 [7]. We isolated neutrophils from patients with chronic

granulomatous disease (CGD) (n=3), who carry NOX2 mutations, rendering them completely deficient in ROS production (Fig S1C). Heme induced similar levels of NETs in CGD and control neutrophils, unlike the phorbol ester PMA, which failed to induce NETs in CGD cells (Fig 2F). Although this oxidase was not involved, heme-induced NETs required ROS signaling since treatment with the ROS scavenger pyrocatechol (Fig S1C) completely abolished NETosis (Fig 2G), suggesting that heme itself might be the oxidizing agent. The requirement for ROS was confirmed with a second scavenger, N-acetyl cysteine (NAC; Fig. S1E). Heme required intracellular oxidant production, since a combination of two non-cell permeant scavengers, catalase and superoxide dismutase, failed to block NETs, as did a scavenger of mitochondrial ROS (Fig. S1E).

In addition to oxidants, heme-triggered NETs required activity of protein kinase C (PKC) [42], cyclin dependent kinase 6 (CDK6) [5], and NE/PR3 [9] but were independent of peptidyl arginine deiminase 4 (PAD4)-mediated citrullination [43] (Fig 2G). We also tested the requirement for *de novo* protein synthesis using the translational inhibitor cycloheximide. This drug, at a concentration that fully blocked synthesis of the cytokine IL-8 (Fig. S1B), had no effect on NET formation (Fig 2G), as previously reported for other NET stimuli [44].

To genetically confirm the role of proteases in heme NET induction, we purified peritoneal neutrophils from NE single and NE/PR3 double knockout mice. NE/PR3 -/- neutrophils failed to release extracellular chromatin, while NE -/- cells displayed a partial deficiency (Fig. 2H & I), demonstrating that these proteases have an essential non-redundant function in decondensing chromatin. In contrast, there was no difference in NET formation between PAD4 -/- and control neutrophils (Fig 2H & I).

**NET fragments drive malaria pathology *in vivo***

To address the function of NETs in *Plasmodium* infections *in vivo*, we used NE/PR3 -/- mice as a NET deficient model. Additionally, to investigate the effect of a failure to degrade NETs extracellularly we used DNase 1 -/- mice. In the absence of DNase 1, NETs are made normally (Fig. 2H & I) but they persist at sites of release because they are not processed into soluble components [4]. DNase 1 -/- animals are deficient in dispersal of NET components and are a model to study the systemic effects of NET-associated alarmins.

We infected mice with the erythrocytic stages of *P. chabaudi*, a rodent malaria parasite that causes a non-lethal, two-week acute infection. Similarly to *P. falciparum, P. chabaudi* iRBCs synchronously sequester in organs and induce pathology [45, 46], although the sequestration pattern differs and cytoadhesion is mediated by different parasite-encoded proteins in the two species. We quantified NETs in plasma by detecting soluble complexes of DNA and the granule protein myeloperoxidase (MPO). We chose MPO over NE in order to enable us to analyze NETs in NE deficient mice. NET components (Fig 3A) and extracellular nucleosomes (Fig. 3B) increased in infected WT mice but were completely absent in NE/PR3 and DNase 1 -/- mice. This result is consistent with a failure to produce NETs in the case of NE/PR3 -/- animals and with a failure to break down the NET macrostructure in the case of DNase 1 -/-. Notably, parasitemia was similar in all three mouse strains (Fig. 3C), showing that NETs are not antiparasitic. As previously described [28, 45], parasitemia peaked between day 9 and 11 and was suppressed by day 13 post infection.

*P. chabaudi* sequesters in the liver and lungs where it induces tissue damage and immunopathology [45]. Livers from WT mice were severely darkened and discolored because of the accumulation of hemozoin and hepatocyte death (Fig. 3D). Remarkably, livers of infected NE/PR3 -/- and DNase 1 -/- mice were completely unaffected and indistinguishable from uninfected controls (Fig. 3D). Livers of WT, but

not NE/PR3 or DNase1 -/- mice, showed necrosis and immune infiltration, characteristic malaria pathology, upon histological analysis of haematoxylin and eosin (H&E) stained sections (Fig. 3E and Fig. S2A and B). We confirmed the liver pathology in wild type, but not mutant mice, with the hepatic damage marker asparate aminotransferase (AST) in plasma (Fig. 3F). Tissue damage was also reduced in lungs of NE/PR3 knockout mice (Fig. S3) compared to WT controls, although *P. chabaudi* causes only mild lung pathology [45]. Altogether, these data demonstrate that release of components from NETs promotes organ pathology in malaria.

**Exogenous NET components restore pathology in NET-deficient mice**

To confirm that NETs are pathogenic in malaria, we injected mice with *in vitro* generated NET fragments. We chose NE/PR3 -/- as the NET-deficient strain in which to carry out this complementation experiment. We first purified peritoneal neutrophils from WT mice and induced them to form NETs. After washing, NETs were dislodged by scraping and sonicated to obtain fragments, which were quantified based on DNA content and injected into the tail vein of control and *P. chabaudi* parasitized mice. Injection of NET fragments did not cause liver pathology in uninfected mice (Fig 3G) nor affect parasitemia in any of the infected genotypes (Fig. S4). Strikingly, restoring NET fragments in parasitized NE/PR3 -/- mice fully recapitulated the liver damage observed in WT mice (Fig 3G). This result demonstrates the direct pathogenicity of NETs and rules out a cell-intrinsic effect of proteases as the cause of the protective effect in the knockout animals.

NETs contain multiple components with inflammatory activity [47]. These include the DNA backbone, as well as the protein fraction that contains many alarmins. Furthermore, extracellular nucleosomes and histones, which form a major portion of NETs, are inflammatory when found in the blood stream [48]. To identify which NET

components are responsible for inducing pathology, we used recombinant DNase 1 to fully digest the DNA of the *in vitro* NET preparation, leaving only the protein components. Notably, the NET protein fraction was sufficient to induce liver damage in NE/PR3 null mice (Fig 3G). As a control, we also injected mouse nucleosomes purified from bone marrow derived macrophages, which failed to induce AST release after injection (Fig 3G). These data show that the pathogenic activity derives from a NET-associated protein .

**NETs induce emergency granulopoiesis via GCSF induction**

Neutrophils cause tissue destruction due to the cytotoxic molecules they carry. We quantified neutrophil infiltration into the livers of parasitized mice using immunofluorescence staining of the intracellular neutrophil marker calgranulin A. Neutrophils accumulated in the livers of WT, but not NE/PR3 and DNase 1 -/- animals (Fig 4A and Fig. S5), consistent with neutrophils being initiators of hepatic pathology.

We quantified systemic neutrophil numbers to determine why both deficient mice genotypes failed to recruit neutrophils into the liver. In malaria, like other infections, the number of circulating neutrophils increases due to emergency granulopoiesis in the bone marrow [49-51]. We observed that *P. chabaudi* infection leads to neutrophilia in WT mice but not in NE/PR3 and DNase1 knockouts (Fig 4B).

The major mediator of emergency granulopoiesis is GCSF [52]. We speculated that NETs directly induce GCSF. To test this, we stimulated macrophages – a significant physiological source of this cytokine - with NETs *in vitro*. NETs robustly induced production of GCSF in human monocyte-derived macrophages, at levels similar to those obtained with bacterial lipopolysaccharide (LPS) and exceeding those obtained with TNF or hemozoin (Fig 4C).

In *P. chabaudi* infected WT mice, the concentration of GCSF in plasma increased with rising parasitemia; however, there was no increase in either NE/PR3 or DNase 1 -/- mice (Fig 4D). To directly demonstrate that NETs induce GCSF *in vivo*, we injected sonicated NETs as described before. Injection of NET fragments fully restored GCSF production in NE/PR3 mice to levels seen in WT mice (Fig 4E). As with the liver damage marker AST, GCSF production was induced by the protein component of NETs, as complete removal of DNA prior to injection did not abrogate the effect. These data show that NET-associated alarmins drive emergency hematopoiesis by inducing GCSF release.

**NETs promote parasite sequestration in organs**

Malaria pathology is linked to parasite sequestration in the microvasculature of afflicted organs. The lack of discoloration in livers of infected NE/PR3 and DNase 1 -/- mice (Fig 3D) suggests a lack of parasite adhesion. To directly analyze sequestration, we infected mice with a luciferase-expressing strain of *P. chabaudi* [45] and quantified sequestered parasite load in organs, at time of maximal cytoadhesion, after perfusing animals to remove unbound, freely-circulating parasites.

As reported, *P. chabaudi* sequestered most prominently in the liver and the lung and, to a lesser degree, in the kidneys [45]. Remarkably, there were tenfold fewer parasites sequestered in the livers and lungs of NE/PR3 and DNAse 1 -/- mice compared to WT controls (Fig 5A). We confirmed this sequestration pattern by histological enumeration of iRBCs in the liver microvasculature (Fig. 5B and Fig. S2B) as well as by electron microscopy (Fig. S2C).

**NETs induce upregulation of endothelial cytoadhesion receptors**

346 The difference in abundance of neutrophils in livers of WT and knockout animals was
347 greater than the difference observed in peripheral blood, indicating that, in addition to
348 emergency granulopoiesis, NETs regulate neutrophil trafficking. Interestingly, both
349 neutrophils [53] and parasites [54, 55] can use the same receptor to dock to
350 endothelial cells: intercellular adhesion molecule 1 (ICAM-1). We hypothesized that
351 NET components regulate expression of ICAM-1 on the endothelium. To test this, we
352 analysed ICAM-1 immunofluorescence in liver sections and observed upregulation
353 on endothelia of infected WT but not NE/PR3 or DNase1 -/- mice, coinciding with the
354 onset of liver damage (Fig. 5C and D). We also measured soluble ICAM-1 in plasma
355 as an additional readout for expression of this receptor, and found no induction in
356 NE/PR3 -/- compared to WT animals (Fig. 5E), confirming our microscopy results.
357 Injection of *in vitro* generated NET fragments into parasitized NE/PR3 -/- mice
358 restored the expression of ICAM-1 (Fig. 5E), demonstrating that NET components
359 control ICAM-1 expression.
360 Parasitized erythrocytes can bind to multiple endothelial surface proteins.
361 Another prominent cytoadhesion receptor is CD36 [56]. We tested if NETs control
362 expression of CD36 by microscopically analyzing protein abundance in lung
363 endothelia. Similarly to ICAM-1, CD36 immunofluorescence increased in lungs of
364 infected mice and this induction was absent in NE/PR3 -/- animals (Fig. 5F). We
365 confirmed this result by quantifying levels of CD36 in plasma (Fig. 5G). Interestingly,
366 and contrary to what we observed with ICAM-1, injection of NETs into uninfected
367 mice was sufficient to upregulate CD36 (Fig 5F). In summary, NET-associated
368 proteins facilitate iRBC sequestration by inducing endothelial activation.
369
370 **Neutralizing GCSF antibodies decrease liver damage**

To test whether GCSF-induced neutrophilia is pathogenic, we neutralized the effects of this cytokine by injected parasitized animals with an anti-GCSF antibody, at day 7 post infection. As expected, the neutralizing antibody did not impact parasite burden (Fig. 6A) but it decreased circulating neutrophils compared to the isotype control (Fig. 6B). This also significantly reduced circulating NET components (Fig 6C), as well as neutrophil trafficking into the liver (Fig. 6D). GCSF neutralization diminished both parasite sequestration (Fig. 6E) and liver damage (Fig. 6F), providing a proof of principle that neutrophils can be successfully targeted in *Plasmodium* infection. Notably, the GCSF concentration in plasma of malaria patients is significantly increased in infected individuals (Fig 6G), as previously reported [57].

## Discussion

Malaria pathophysiology is based on an interplay of parasite proliferation, host inflammatory response and microvascular obstruction due to binding of iRBCs to activated endothelia. Despite important recent advances [17, 18, 58], the contribution of neutrophils to these processes remains poorly understood. Here we demonstrate that neutrophils play an essential role in both propagation of inflammation and facilitation of parasite cytoadherence.

Firstly, we showed that in malaria, as in sickle-cell disease [40], extracellular heme triggers NETosis in TNF-primed neutrophils. Heme-induced NETs require some of the same signaling intermediates demonstrated for other NET inducers, including neutrophil proteases [8], CDK6 [5] and PKC [42]. Heme was previously shown to activate PKC in neutrophils, initiating chemotaxis and IL-8 production [59]. TNF priming provides a synergistic signal required for NETosis; this signal is posttranslational, since it is not blocked by the translational inhibitor cycloheximide. Heme-induced NETs are independent of the citrullinating enzyme PAD4, which is

implicated in ionophore-induced NETs [43] and of the oxidant-generating enzyme NOX2 [41], which is known to be suppressed in neutrophils from malaria patients [26]. ROS signaling is nevertheless required for heme NETs, as the response is blocked by the ROS scavenger pyrocathecol. This may be due to the fact that heme is itself a redox-active molecule, with multiple mechanisms for initiating and propagating free radicals [60]. In summary, heme utilizes a unique pathway for NET induction that nevertheless requires both protease activity and ROS signaling.

NETs are essential for malaria pathology in the *P. chabaudi* model. We showed that solubilization of NETs by serum Dnase1 liberates immunostimulatory components that diffuse systemically and are pathogenic via two mechanisms. The first is induction of GCSF in macrophages, which initiates emergency granulopoiesis. This corresponds to what is seen in patients, where GCSF is elevated in both *P. falciparum* [57] and *P. vivax* infections [61]. Moreover, neutrophil turnover is often higher in malaria [49-51] and, in children living in endemic areas, increased neutrophil counts correlate with symptoms of severe disease, such as prostration, coma and respiratory distress [62-64]. In a second mechanism, NET components upregulate mouse ICAM-1, a key cytoadhesion receptor that sequesters parasitized RBCs in the microvasculature of both mice and patients [54, 55]. Interestingly, in *P. falciparum* malaria, ICAM-1 mediates cytoadhesion in the brain and is a key mediator of cerebral malaria [55, 65]. Antibodies against ICAM-1 binding variants of *P. falciparum* Erythrocyte Membrane Protein 1 (PfEMP1), the main parasite cytoadhesion factor, protect against clinical disease [66, 67]. NET induction of ICAM-1, which facilitates *P. chabaudi* adhesion in the liver, may thus operate in human malaria to recruit *P. falciparum* iRBCs to the brain, a far more dangerous sequestration site. This is consistent with recent reports showing an association

423 between neutrophil proteins and cerebral malaria [17, 18]. Whether NETs can also
424 upregulate ICAM-1 on human brain endothelium remains to be verified.
425 NET components are also required for pathology and parasite sequestration in the
426 lungs of infected animals, demonstrating that this mechanism may be broadly
427 generalizable to different vascular beds. Furthermore, in the *P. chabaudi* model, lung
428 sequestration is mediated by an unidentified receptor other than ICAM-1 [54],
429 consistent with NET components inducing more than one cytoadhesion molecule. It
430 will be interesting to test if a similar mechanism operates in humans, since
431 neutrophils are known to infiltrate the lungs of malaria patients with acute respiratory
432 distress [68].
433 Our data demonstrate the essential role of DNAse 1 in releasing pathogenic NET
434 fragments in *P. chabaudi* malaria. NETs are thought to be anchored to the
435 endothelium after release [69, 70], through von Willebrand factor [69] and probably
436 other mediators. Serum DNAse 1 allows systemic diffusion of NET components, as
437 demonstrated by absence of NET fragments in DNase 1 knockouts. A similar
438 pathogenic function of DNAse 1 was shown in a polymicrobial sepsis model, where
439 injection of recombinant DNase 1 promotes liver damage and neutrophil
440 accumulation in liver and lung [71]. However, DNase 1 has contradictory roles in
441 inflammation: in thrombosis [72, 73], cancer [74] and SLE [4], this endonuclease is
442 protective rather than pathogenic. In sterile inflammation it is therefore the
443 unprocessed NET 'macrostructure' that is detrimental, while in infections such as
444 malaria and sepsis, it is the discrete molecular components of NETs that cause
445 disease.
446 The NET proteins that induce GCSF and ICAM-1 remain unknown. Many
447 proteins found on NETs are classified as alarmins [75]; including α-defensins,
448 cathelicidin, calgranulin and lactoferrin [76]. Once released, these alarmins can

induce the maturation and activation of dendritic cells, T cells, macrophages and endothelial cells [75]. Additional experiments will determine which NET-bound proteins are responsible for triggering granulopoiesis and endothelial activation.

NET-associated molecules are necessary but not sufficient to drive inflammation in *P. chabaudi* malaria, as shown by the injection of NET fragments into uninfected mice. Additional stimuli, most likely *Plasmodium* PAMPs, are required to initiate emergency hematopoiesis and liver damage. Although parasite proteins and hemozoin did not directly induce NETs, they are known to significantly contribute to immune activation via other pathways [25] . Furthermore, inflammation in malaria is complex, with type-I interferons [28], CD8+ T cells [21, 45] and hemostasis [77] contributing to immunopathogenesis in both mice and humans. Further investigation is required to understand how neutrophils cross talk with other cell types in initiating disease.

Malaria exerts an evolutionary selective pressure on populations living in endemic areas, selecting for gene variants that promote tolerance [78]. Interestingly, people of African descent and some ethnic groups from the Middle East, have low neutrophil counts [79]. This “ethnic or benign neutropenia” could be the result of selective pressure to suppress neutrophil counts since they are detrimental in this disease. Strikingly, in addition to Duffy antigen, the loci linked to ethnic neutropenias include *CDK6* and *GCSF [80]*, both of which are directly involved in the NET-mediated pathogenic mechanism described here.

Recent studies confirmed the central role of heme in the pathophysiology of malaria [81, 82]. Moreover, extracellular heme accumulation is not limited to malaria; it is a confirmed pathogenic factor in sepsis, sickle cell disease, intracerebral hemorrhage and atherosclerosis [60], all of which also have reported neutrophil involvement. It will therefore be interesting to examine if emergency hematopoiesis

475 and endothelial activation triggered by NET fragments are universal outcomes in
476 intravascular hemolytic diseases.
477 Adjunctive therapies that treat the life-threatening complications of malaria are
478 urgently needed. We show that NETs control inflammation and parasite
479 cytoadherence, placing neutrophils at the nexus of malaria pathophysiology and
480 identifying them as a potential target for adjunctive therapy.
481

## Materials and Methods

### Human samples

Our study was conducted in accordance with the Helsinki Declaration. Blood collection from healthy donors and CGD patients was approved by the ethical committee of Charité University Hospital, Berlin, Germany. Collection of blood from malaria patients in Gabon was approved by the Comité d'Ethique Régional Indépendent de Lambaréné in Gabon. All study participants provided written informed consent before being enrolled in the study.

Collection of blood samples from patients in Mozambique was approved by the Bioethical Committee in Mozambique and by the Regional Ethical Committee for Medical and Health Research Ethics in Eastern Norway. This study was previously described [83] and consisted of patients admitted to the Central Hospital of Maputo, Mozambique during two malaria peak seasons, from 2011 to 2012. Inclusion criteria were age ≥ 18 years, non-pregnancy, axillary temperature ≥ 38 °C, confirmed malaria infection, and informed written/fingerprint consent from patient or next of kin.
Ethical approval to obtain, store and use post-mortem human tissue from Malawian children with fatal cerebral malaria and non-CM encephalopathy was obtained from the research ethics committees at the College of Medicine Malawi, Liverpool School of Tropical Medicine and Michigan State University. Informed consent was obtained from the parents or legal guardians of all the children enrolled.

### Chemicals and stimuli

PMA (P8139, Sigma), Heme (H651-9, Frontier Scientific), murine TNF (315-01A, Peprotech), human TNF (300-01A, Peprotech), PKC inhibitor (Go6976, Tocris), pyrocatechol (C9510, Sigma), Hoechst (639, Immunochemistry), cycloheximide

(Sigma), Cdk4/6 inhibitor (LY2835219, Selleck), PAD4 inhibitor (TDFA, Tocris), NE inhibitor (GW311616A, Sigma-Aldrich), Luminol (11050, AAT-Bioquest), horse radish peroxidase (HRP, 31941, Serva), Bright-Glo Luciferase Substrate (E2610, Promega)

**Immunofluorescence microscopy on human retinal tissue**

Paraffin sections (3–4 μm thick) were deparaffinised in two changes of xylene 100% for 5 minutes each and then hydrated in two changes of 100% ethanol for 5 minutes each, 90% and 70% ethanol for 1 minute each. For antigen retrieval UNI-TRIEVE (Universal Mild Temperature Retrieval Solution) was used to incubate the slides at 60$^{o}$C for 30 minutes. Afterwards slides were rinsed in PBS and blocked with Normal Horse serum for 30 minutes. Serum was removed and sections were incubated with primary antibody at appropriate dilution (1:200) in Normal Horse serum overnight at 4 °C. Sections were rinsed in PBS Tween and then incubated with secondary antibody at appropriate concentration (1:400) for ~30 minutes in the dark and then rinsed in PBS Tween for 3 x 5 min before mounting with a DAPI containing medium (VECTASHIELD Antifade Mounting Medium with DAPI Cat. No: H-1200, Vector) which counterstains the nuclei. Primary antibodies for detection of NETs were: Neutrophil Elastase Antibody (G-2), (sc-55549; Santa Cruz) and Anti-Histone H3 Antibody (citrulline R2 + R8 + R17) (ab5103; Abcam). Secondary antibodies were: Goat Anti-Rabbit IgG H&L Alexa Fluor® 488 (Abcam; ab150081) and Goat Anti-Mouse IgG H&L Alexa Fluor® 594 (Abcam; ab150116).

Inverted Widefield Microscope (WF1-Zeiss) with LED illumination Zeiss Axio Observer and the highly sensitive Hamamatsu Flash 4 camera were used for fluorescent imaging. Z-stack images were collected at 63X magnification. Fiji and ICY [84] were

used for 3D visualization of z stack images. Huygens software was used for deconvolution of z-stack images.

**NETs ELISA**

NETs in plasma were determined as NE/DNA complexes in human samples and MPO/DNA complexes in mouse samples. For the human ELISA we used the precoated and blocked plates of the Hycult human NE ELISA (HK319-02). Undiluted plasma samples (50 µl) were incubated for 2h at room temperature with 350 rpm agitation and washed three times with PBS-0.05% Tween (PBS-T). The anti-DNA-POD antibody (Cell Death Detection ELISA Kit, Roche) was diluted 1:100, and the plate was incubated for 2h at room temperature, followed by five washes with PBS-T and incubation with TMB substrate. Signal was acquired at 450 nm.

For the mouse ELISA, the biotinylated primary mouse anti-MPO antibody (1µg/ml final concentration, HM1051BT, Hycult ) was coated onto a streptavidin coated plate from the Cell Death Detection ELISA Kit (Roche) at 4°C overnight, followed by three washes with PBS-T. The plates were subsequently blocked for 2h with 1 % BSA in PBS and 50 µl undiluted mouse serum was added to wells. The plate was incubated for 2h at room temperature with agitation (300 rpm on a plate shaker), followed by three washes with PBS-T and addition of 50 µl per well of anti-DNA-POD from Roche cell death ELISA kit (1:100). The plate was incubated for two hours with agitation at room temperature, washed five times with PBST and developed with ABTS.

**ELISA Kits**

The following kits were used for plasma quantifications, according to manufacturer's instructions: Cell Death Detection ELISA Plus (11920685001, Roche Diagnostics), Human Interleukin 8 Quantikine ELISA (S8000C, R&D Systems), mouse GCSF

559 Quantikine ELISA (MCS00, R&D Systems), human GCSF Quantikine ELISA (SCS50,
560 R&D Systems), mouse ICAM-1 ELISA (DY796, R&D Systems), mouse CD36 ELISA
561 (EMCD36, ThermoFisher)
562
563 **Human neutrophil isolation and stimulation**
564 Cells were purified by a first centrifugation of whole blood over Histopaque-1119
565 (Sigma) followed by a discontinuous Percoll (Sigma) gradient [85]. All experiments
566 were done in RPMI-1640 (w/o phenol red, Gibco) supplemented with 10mM HEPES
567 and 0.05% human serum albumin (Albutein, Grifols). For NET induction, $10^5$
568 neutrophils were seeded onto glass coverslips in a 24 well plate and incubated with
569 inhibitors for 30 min, followed by 15 min priming with TNF and addition of the stimuli.
570
571 **Luminol assay**
572 To assess ROS production, $1x10^5$ neutrophils were activated (after treatment with
573 inhibitors/ROS scavengers) with 50 nM PMA. ROS production was measured by
574 monitoring luminol (50 µM) luminescence in the presence of 1.2U/ml horseradish
575 peroxidase [85].
576
577 **Mice**
578 Mouse breeding, infections and isolation of peritoneal neutrophils were approved by
579 the Berlin state authority *Landesamt für Gesundheit und Soziales*. Animals were bred
580 at the Max Planck Institute for Infection Biology. Mice were housed in specific pathogen
581 free (SPF) conditions, maintained on a 12-hour light/dark cycle and fed *ad libitum*.
582 NE -/- [86], NE/PR3 -/- [87] and DNase 1 -/- [88] mice were previously described. PAD4
583 -/- mice [89] were a kind gift of Denisa Wagner.
584

585 **Mouse neutrophil isolation and stimulation**

586 Murine neutrophils were isolated from peritoneal cavities after elicitation with casein
587 (Sigma) and centrifugation over Percoll as previously described [90].
588 Cells were seeded onto glass coverslips at $10^5$/well in 24 well plates in RPMI (Gibco)
589 containing penicillin/streptomycin (Gibco) and glutamine (Gibco), 1% murine DNase 1
590 -/- serum and 100 ng/ml murine G-CSF (Peprotech). After 30 min equilibration and 15
591 min TNF priming, cells were stimulated with 100 nM PMA or 20 µM heme. NETs were
592 quantified after 15 hours stimulation as described below.
593

594 **Quantification of NET formation**
595
596 The quantification of NETosis was carried out as previously described [91]. Briefly,
597 cells were fixed for 30 minutes at room temperature in 2 % paraformaldehyde (PFA),
598 permeabilized with 0.5 % Triton-X100 and blocked for 30 minutes in blocking buffer.
599 Cells were then stained with the anti-neutrophil elastase antibody (Calbiochem
600 481001, 1:200) and an antibody directed against the nucleosomal complex of Histone
601 2A, Histone 2B and chromatin (PL2/3; 1 ug/ml) [92], as well as the secondary
602 antibodies goat anti-mouse Alexa Fluor 568 (1:500), goat anti-rabbit Alexa Fluor 488
603 (1:500) and Hoechst 33342 (Sigma-Aldrich). Samples were mounted on coverslips
604 with Mowiol. Image acquisition was done using a Leica DMR upright fluorescence
605 microscope equipped with a Jenoptic B/W digital microscope camera and analyzed
606 using ImageJ/FIJI software.
607

608 **Heme preparation**

609 Heme for *in vitro* stimulation of neutrophils and for standard curve was prepared fresh
610 on the day of the experiment. A 10 mM stock solution was prepared by dissolving

611 0.0325 g Hemin (H651-9, Frontier Scientific) in 5 ml DMSO. An intermediate 1:10
612 dilution in PBS was made before stimulating the cells.
613
614 **Quantification of plasma heme**
615
616 Heme was quantified using the formic acid assay [93]. Briefly, samples were diluted
617 1:50 in $H_2O$ in white 96 well plates. The heme concentration was determined after the
618 addition of 100% formic acid (150 µL/well, Merck) to all samples and absorbance
619 measurement at 405nm using a microplate reader. Measurements were compared to
620 a hemin standard curve in the range of 0.25 – 16 µM in $H_2O$.
621
622 ***P. falciparum*** **culture**
623 *P. falciparum* parasites were cultured using standard procedures as described
624 previously [94] . Parasites were grown at 5% hematocrit in RPMI 1640 medium, 0.5%
625 AlbuMax II (Invitrogen), 0.25% sodium bicarbonate, and 0.1 mg/ml gentamicin.
626 Cultures were incubated at 37°C in an atmosphere of 5% oxygen, 5% carbon dioxide,
627 and 90% nitrogen.
628
629 **Trophozoite and merozoite preparation**
630 A late stage *P. falciparum* culture was washed and taken up in 2 ml of RPMI and
631 layered onto 5 ml of a 60% Percoll solution. The mixture was centrifuged at 2000 xg
632 for 20 minutes at 20ºC and trophozoites were collected at the interphase between
633 RPMI and Percoll, while uninfected RBCs and ring stage infected RBCs were pelleted.
634 Parasites were washed three times with RPMI and iRBCs were pelleted. For merozoite
635 isolation iRBCs were lysed with 0.03 % saponin solution. Subsequently the sample
636 was washed three times with PBS and taken up in RPMI. Concentration of merozoites
637 was determined by use of a Neubauer chamber.

638

639 **Isolation of digestive vacuoles from *P. falciparum***

640 Late trophozoite cultures with 10 % parasitemia were allowed to complete schizogony
641 and reinfection. Cultures were stratified on a discontinuous Percoll-mannitol gradient
642 and expelled digestive vacuoles collected on the 10/40 % Percoll interphase as
643 described [95]. The collected interphase was passed through a 27 G needle and
644 separated by density using 42 % Percoll. The intact DVs could be collected as dark-
645 grey colored bottom fraction. DVs were resuspended in uptake buffer (pH 7.4, 2mM
646 $MgSO_4$, 100 mM KCl, 25 mM HEPES, 25 mM $NaHCO_3$ and 5mM $Na_3PO_4$), washed
647 and used in subsequent experiments.

648

649 ***P. chabaudi* infections, plasma and tissue preparation**

650 Male mice aged 8-15 weeks were infected by intravenous injection of viable *P.*
651 *chabaudi* AS parasites (WT) or PccASluc (luciferase-expressing; [45]). To ensure
652 viability of the parasites, a frozen aliquot was thawed and injected intraperitoneally into
653 a transfer mouse. The number of asexual parasites intravenously injected into each
654 mouse was adjusted according to body weight so that every animal received $1x10^4$
655 iRBCs per 20 grams. Parasitemia was monitored from day 5 post infection every 48
656 hours by Giemsa-stained thin blood smear. Anti-GCSF antibody (150 µl per mouse,
657 R&D) or isotype control (150 µl per mouse, R&D) were injected intravenously on day
658 7 post infection.

659 Mice were bled by cardiac puncture under non-recovery deep anesthesia. Blood was
660 kept from coagulating by addition of 50 µM final concentration of EDTA (Sigma).
661 Plasma was generated by centrifugation at 10,000 x g at 4°C for 10 minutes. Plasma
662 was aliquoted, snap frozen in liquid nitrogen and stored at -80°C until further use.
663 Plasma was always thawed on ice.

664 Organs were harvested without additional perfusion (except in parasite sequestration
665 experiments) as blood was removed by terminal bleeding of the animals. The organs
666 were fixed for 20h at room temperature in 2% PFA.
667
668 **Immunohistochemistry**
669
670 The blinded scoring of liver pathology as well as the counting of parasites sequestered
671 in the microvasculature of the livers was performed by trained pathologists at the
672 iPATH-Berlin Core Unit for immunopathology of experimental model organisms from
673 H&E stained Paraffin sections of 1 µm thickness.
674 The scores were defined as follows:

Hepatitis (Malaria)

The following score sheet was modified from [96]**.** Each of the scored findings was judged individually and assigned a score. The value plotted for each animal is the sum of all individual scores.

| **Histopathologic changes** | **Histopathologic grading** | | | |
|---|---|---|---|---|
| | **0** | **1** | **2** | **3** |
| Fatty change | No fatty change | < 10% | 10-50% | > 50% |
| Kupffer cells/HPF | < 20/HPF | 20-35/HPF | 36-50/HPF | > 50/HPF |
| Portal tract inflammation | < 5% of portal tract area | 5-15% of portal tract area | 16-30% of portal tract area | > 30% of portal tract area |
| Bile duct proliferation | No proliferation | Mild proliferation | Moderate proliferation | Severe proliferation |
| Sinusoid congestion | No congestion | Mild congestion | Moderate congestion | Severe congestion |
| Haemozoin deposition | No deposition | Mild deposition | Moderate deposition | Severe deposition |
| Necrosis | none | <10% | 11-25% | >25% |

675
676
677

678 **Acute Lung injury**

679 The following score sheet was modified from [97]. Animals were assigned to

680 individual categories matching their histopathological signs.

681
682

| |
|---|
| **0**: thin and delicate alveolar septae, no intra-alveolar fibrin strands or hyaline membranes and <5 intra-alveolar cells, no perivascular or peribronchial infiltrates |
| **1**: mildly congested alveolar septae, few fibrin strands or hyaline membranes and <10 intra-alveolar cells with mild perivascular and/or peribronchial infiltration |
| **2**: moderately congested alveolar septae, some fibrin strands or hyaline membranes, <20 intra-alveolar cells with moderate perivascular and/or peribronchial infiltration |
| **3**: severely congested alveolar septae, many fibrin strands and presence of hyaline membranes, >20 intra-alveolar cells with severe perivascular and/or peribronchial infiltration |

683
684
685 **Immunofluorescence of mouse tissue sections**
686
687 Mouse tissue were fixed in 2% paraformaldehyde solution in Tris-buffered saline (TBS,

688 pH 7.4) for 20 hours at room temperature. The tissue was then dehydrated and

689 paraffin-embedded (60°C) using a Leica TP 1020 tissue processor.

690 Paraffin blocks were cut to 3 µm and sections were mounted and dried on Superfrost

691 Plus slides (Thermo Scientific) avoiding temperatures above 37°C. After dewaxing and

692 rehydration, sections were incubated in HIER buffer pH6 (citrate buffer) [20 minutes at

693 96°C in a steam cooker (Braun)].

694 After antigen retrieval, sections were left in the respective HIER buffer at room

695 temperature to cool below 30°C, rinsed three times with deionized water and once with

696 PBS pH 7.4, and permeabilized for five minutes with 0.5% Triton-X100 in PBS at room

697 temperature, followed by three rinsing steps with PBS.

698 Sections were surrounded with PAP-pen and treated with blocking buffer for 30

699 minutes to prevent non-specific binding. Primary antibodies were diluted in blocking

buffer and incubated on the sections overnight at room temperature. The following primary antibodies were used for tissue sections: anti-mouse-ICAM (AF796, Novus Biologicals, dilution 1:200), anti-mouse-Calgranulin (MPIIB, in house [5], dilution 1:50) and anti-CD36 (NB400-144, Novus, 1:200). We used secondary antibodies raised in donkey and pre-absorbed against serum proteins from multiple host species (Jackson Immuno Research). Dilution and blocking was done in PBS supplemented with 1% BSA, 2% donkey normal serum, 5% cold water fish gelatin, 0.05% Tween 20 and 0.05% Triton X100.

Slides were mounted using Mowiol and digitized with a ZEISS AxiosScan.Z1. This is an automated microscope that generates a series of overlapping photographs which are assembled to a single image of a complete organ section, in an operator independent manner. The relative abundance of CalgA (neutrophils), ICAM-1 or CD36 was then calculated by normalizing the respective pixels to the DAPI pixels (total tissue area), using the software package Volocity 6.3.

**Determination of liver enzyme concentration in mouse plasma**

The concentration of the hepatocyte specific enzyme aspartate-aminotransferase in the plasma of experimental animals were determined by the routine veterinarian service laboratory at SYNLAB.vet GmbH (Berlin, Germany).

**FACS analysis of mouse whole blood**

100 µl of mouse whole blood were stained directly by addition of 100 µl of FACS antibodies diluted 1:100 in FACS buffer (PBS supplemented with 2.5 % FCS and 0.1 % $NaN_3$) for 30 minutes. Cells were treated with 3 ml 1-Step Fix/Lyse (00-5333-54, eBioscience) for 60 min at room temperature, washed once as per manufacturer's

instructions and taken up in 250 µl FACS buffer prior to analysis using a MACSQuant Analyser.

Antibodies were all from BD Biosciences: V500 anti-CD45 (561487), FITC anti-CD3(561798), PE anti-CD115 (565249), PerCP-Cy5.5 anti-Ly6G/C (561103). Neutrophils were defined as CD45+, CD115-, Ly6G/C+.

**Assessment of sequestration of luciferase-expressing parasites**

Mice were infected with a luciferase-expressing strain of *P. chabaudi* (PccASluc [45]) as described above but kept on a reverse light cycle, as sequestration occurs during the dark cycle [45]. At the time of maximum sequestration (12.00 – 14.00 h coordinated universal time (UCT), reverse light) mice were sacrificed and perfused systemically by injection of 10 ml PBS into the heart. Organs were harvested and 0.1 g of tissue was transferred to a Precellys homogenizer tube in PBS and dissociated for one cycle, 10 seconds at 4500 rpm in a Precellys Evolution Homogenizer. The sample was then diluted 1:10 in PBS, and an equal volume (100 µL) of Bright-Glo substrate (Promega) was added. Luciferase activity was measured after 2 min incubation using a Perkin Elmer VICTOR X Light Multilabel Plate Reader.

**Injection of exogenous NETs and control chromatin**

Murine NETs were prepared from WT peritoneal neutrophils with PMA as described above, washed three times with PBS to remove residual PMA, scraped from the plate and sonicated for 15 seconds at 70% Power using a Bandelin SONOPLUS sonicator. DNA concentration was quantified by PicoGreen assay (P11496, Thermo Fisher Scientific) or NanoDrop measurements . For removal of DNA, the sample was then treated with 2 U DNase1 from TURBO DNA-free Kit (AM1907, ThermoFisher Scientific) overnight at 37°C. The kit was chosen because it contains a DNase

753 inactivating agent, which was used according to manufacturer's specifications to
754 ensure that no DNase activity was introduced into injected mice. Complete digestion
755 of DNA was confirmed both by agarose gel electrophoresis and PicoGreen
756 measurement. Mice were injected with an amount of NETs and chromatin previously
757 observed to have accumulated in infected WT mice, which was 300 ng/ml of blood.
758 We assumed a blood volume of an adult male mouse of 1.5 ml and therefore injected
759 450 ng of either NETs or chromatin into each mouse.
760
761 Control chromatin was isolated from bone marrow derived macrophages, which were
762 prepared according to standard protocol [98]. Chromatin was prepared as previously
763 described [99]. Briefly, when cells were confluent they were harvested, washed and
764 counted. 300 µl of hypotonic buffer A (10 mM HEPES, pH 7.5, 10 mM KCl, 3 mM NaCl,
765 3mM $MgCl_2$, 1 mM EDTA, mM EGTA and 2 mM dithiothreitol and a general protease
766 inhibitor cocktail (78430, ThermoFisher Scientific)) was added per $5x10^6$ cells and
767 incubated on ice for 15 minutes. Subsequently 0.05 volumes of 10 % Nonidet P-40
768 were added, the cells were vortexed and centrifuged at 500 x g for 10 minutes at 4°C.
769 The supernatant was discarded, the nuclei in the pellet washed in buffer A and
770 subsequently resuspended in 50 µl of ice-cold buffer NE (20 mM HEPES, pH 7.5, 25
771 % glycerol, 0.8 mM KCl, 1mM $MgCl_2$, 1 % Nonidet P-40, 05. mM EDTA, 2 mM
772 dithiothreitol). Following a 20 minutes incubation on ice with occasional mixing the
773 samples were centrifuged at 14,000 x g for 15 minutes at 4°C. The supernatant was
774 discarded and the pellet containing the chromatin resuspended in $ddH_2O$. Chromatin
775 concentration was determined by Picogreen assay (see above) and samples were
776 stored at -80°C.
777
778 **Macrophage stimulation with NETs**

Monocytes were isolated by magnetic CD14 positive selection (130-050-201, Miltenyi Biotec) and differentiated for 7 days into macrophages in RPMI 1640 containing penicillin/streptomycin, glutamine and 5 ng/ml human MCSF. At the day of the experiment, $3x10^6$ neutrophils were stimulated for 4 h with 50 nM PMA. The resulting NETs were washed three times with PBS, harvested by scraping and sonicated. The NET concentration was determined by Picogreen assay. Macrophages were stimulated for 12 h with 1 µg/ml isolated NETs, 100 µg/ml hemozoin (Sigma), 2 ng/ml TNF (Peprotech) or 100 ng/ml LPS from Salmonella (Enzo Life Sciences).

**List of Supplementary Materials**

Supplementary Figure 1: *in vitro* stimulations of human neutrophils

Supplementary Figure 2: Necrosis and sequestration in the livers of *P. chabaudi* infected mice.

Supplementary Figure 3: Pathology in the lungs of *P. chabaudi* infected animals.

Supplementary Figure 4: Parasitemia of NET fragment injected mice.

Supplementary Figure 5: Immunofluorescence images used to quantify neutrophils in livers of infected mice.

Table S1: Gabon uncomplicated malaria cohort patient information.

Table S2: Gabon severe malaria cohort patient information.

Table S3: Mozambiqe severe malaria cohort patient information.

## References and Notes:


1. Amulic, B., et al., *Neutrophil function: from mechanisms to disease.* Annu Rev Immunol, 2012. **30**: p. 459-89.
2. Brinkmann, V., et al., *Neutrophil extracellular traps kill bacteria.* Science, 2004. **303**(5663): p. 1532-5.
3. Papayannopoulos, V., *Neutrophil extracellular traps in immunity and disease.* Nat Rev Immunol, 2018. **18**(2): p. 134-147.
4. Hakkim, A., et al., *Impairment of neutrophil extracellular trap degradation is associated with lupus nephritis.* Proc Natl Acad Sci U S A, 2010. **107**(21): p. 9813-8.
5. Amulic, B., et al., *Cell-Cycle Proteins Control Production of Neutrophil Extracellular Traps.* Dev Cell, 2017. **43**(4): p. 449-462.e5.
6. Hakkim, A., et al., *Activation of the Raf-MEK-ERK pathway is required for neutrophil extracellular trap formation.* Nat Chem Biol., 2011. **7**(2): p. 75-7. doi: 10.1038/nchembio.496. Epub 2010 Dec 19.
7. Fuchs, T.A., et al., *Novel cell death program leads to neutrophil extracellular traps.* J Cell Biol., 2007. **176**(2): p. 231-41. Epub 2007 Jan 8.
8. Papayannopoulos, V., et al., *Neutrophil elastase and myeloperoxidase regulate the formation of neutrophil extracellular traps.* J Cell Biol., 2010. **191**(3): p. 677-91. doi: 10.1083/jcb.201006052. Epub 2010 Oct 25.
9. Warnatsch, A., et al., *Inflammation. Neutrophil extracellular traps license macrophages for cytokine production in atherosclerosis.* Science., 2015. **349**(6245): p. 316-20. doi: 10.1126/science.aaa8064. Epub 2015 Jul 16.
10. Sollberger, G., et al., *Gasdermin D plays a vital role in the generation of neutrophil extracellular traps.* Sci Immunol, 2018. **3**(26).
11. Kessenbrock, K., et al., *Proteinase 3 and neutrophil elastase enhance inflammation in mice by inactivating antiinflammatory progranulin.* J Clin Invest, 2008. **118**(7): p. 2438-47.
12. Thanabalasuriar, A., et al., *Neutrophil Extracellular Traps Confine Pseudomonas aeruginosa Ocular Biofilms and Restrict Brain Invasion.* Cell Host Microbe, 2019. **25**(4): p. 526-536.e4.
13. Smith, C.K. and M.J. Kaplan, *The role of neutrophils in the pathogenesis of systemic lupus erythematosus.* Curr Opin Rheumatol, 2015. **27**(5): p. 448-53.
14. Silvestre-Roig, C., et al., *Externalized histone H4 orchestrates chronic inflammation by inducing lytic cell death.* Nature, 2019. **569**(7755): p. 236-240.
15. Schreiber, A., et al., *Necroptosis controls NET generation and mediates complement activation, endothelial damage, and autoimmune vasculitis.* Proc Natl Acad Sci U S A, 2017. **114**(45): p. E9618-e9625.
16. Martinod, K. and D.D. Wagner, *Thrombosis: tangled up in NETs.* Blood, 2014. **123**(18): p. 2768-76.
17. Feintuch, C.M., et al., *Activated Neutrophils Are Associated with Pediatric Cerebral Malaria Vasculopathy in Malawian Children.* MBio, 2016. **7**(1): p. e01300-15.
18. Lee, H.J., et al., *Integrated pathogen load and dual transcriptome analysis of systemic host-pathogen interactions in severe malaria.* Sci Transl Med, 2018. **10**(447).
19. Ghebreyesus, T.A. and K. Admasu, *Countries must steer new response to turn the malaria tide.* Lancet, 2018. **392**(10161): p. 2246-2247.
20. Miller, L.H., et al., *Malaria biology and disease pathogenesis: insights for new treatments.* Nature medicine, 2013. **19**(2): p. 156.

21. Deroost, K., et al., *The immunological balance between host and parasite in malaria.* FEMS Microbiol Rev, 2016. **40**(2): p. 208-57.
22. Deitsch, K.W. and R. Dzikowski, *Variant Gene Expression and Antigenic Variation by Malaria Parasites.* Annu Rev Microbiol, 2017. **71**: p. 625-641.
23. Wassmer, S.C. and G.E. Grau, *Severe malaria: what's new on the pathogenesis front?* Int J Parasitol, 2017. **47**(2-3): p. 145-152.
24. Grau, G.E. and A.G. Craig, *Cerebral malaria pathogenesis: revisiting parasite and host contributions.* Future Microbiol, 2012. **7**(2): p. 291-302.
25. Gazzinelli, R.T., et al., *Innate sensing of malaria parasites.* Nat Rev Immunol, 2014. **14**(11): p. 744-57.
26. Cunnington, A.J., et al., *Prolonged neutrophil dysfunction after Plasmodium falciparum malaria is related to hemolysis and heme oxygenase-1 induction.* J Immunol, 2012. **189**(11): p. 5336-46.
27. Bostrom, S., et al., *Neutrophil alterations in pregnancy-associated malaria and induction of neutrophil chemotaxis by Plasmodium falciparum.* Parasite Immunol, 2017. **39**(6).
28. Rocha, B.C., et al., *Type I Interferon Transcriptional Signature in Neutrophils and Low-Density Granulocytes Are Associated with Tissue Damage in Malaria.* Cell Rep, 2015. **13**(12): p. 2829-2841.
29. Lin, J.W., et al., *Signatures of malaria-associated pathology revealed by high-resolution whole-blood transcriptomics in a rodent model of malaria.* Sci Rep, 2017. **7**: p. 41722.
30. Chen, L., Z. Zhang, and F. Sendo, *Neutrophils play a critical role in the pathogenesis of experimental cerebral malaria.* Clin Exp Immunol, 2000. **120**(1): p. 125-33.
31. Sercundes, M.K., et al., *Targeting Neutrophils to Prevent Malaria-Associated Acute Lung Injury/Acute Respiratory Distress Syndrome in Mice.* PLoS Pathog, 2016. **12**(12): p. e1006054.
32. Gillrie, M.R., et al., *Plasmodium falciparum Histones Induce Endothelial Proinflammatory Response and Barrier Dysfunction.* Am J Pathol, 2012. **180**(3): p. 1028-39.
33. Baker, V.S., et al., *Cytokine-associated neutrophil extracellular traps and antinuclear antibodies in Plasmodium falciparum infected children under six years of age.* Malar J, 2008. **7**: p. 41.
34. Kho, S., et al., *Circulating neutrophil extracellular traps and neutrophil activation are increased in proportion to disease severity in human malaria.* J Infect Dis, 2018.
35. Kun, J.F., et al., *Merozoite surface antigen 1 and 2 genotypes and rosetting of Plasmodium falciparum in severe and mild malaria in Lambarene, Gabon.* Trans R Soc Trop Med Hyg, 1998. **92**(1): p. 110-4.
36. *WHO. Guidelines for the treatment of malaria. Third ed. 2015:76.* http://www.who.int/malaria/publications/atoz/9789241549127/en.
37. Taylor, T.E., et al., *Differentiating the pathologies of cerebral malaria by postmortem parasite counts.* Nat Med, 2004. **10**(2): p. 143-5.
38. Barrera, V., et al., *Neurovascular sequestration in paediatric P. falciparum malaria is visible clinically in the retina.* Elife, 2018. **7**.
39. MacCormick, I.J., et al., *Cerebral malaria in children: using the retina to study the brain.* Brain, 2014. **137**(Pt 8): p. 2119-42.
40. Chen, G., et al., *Heme-induced neutrophil extracellular traps contribute to the pathogenesis of sickle cell disease.* Blood, 2014. **123**(24): p. 3818-27.

41. Kenny, E.F., et al., *Diverse stimuli engage different neutrophil extracellular trap pathways.* eLife, 2017. **6**.
42. Neeli, I. and M. Radic, *Opposition between PKC isoforms regulates histone deimination and neutrophil extracellular chromatin release.* Frontiers in immunology, 2013. **4**: p. 38-38.
43. Martinod, K., et al., *Neutrophil histone modification by peptidylarginine deiminase 4 is critical for deep vein thrombosis in mice.* Proc Natl Acad Sci U S A, 2013. **110**(21): p. 8674-9.
44. Sollberger, G., B. Amulic, and A. Zychlinsky, *Neutrophil Extracellular Trap Formation Is Independent of De Novo Gene Expression.* PLoS One., 2016. **11**(6): p. e0157454. doi: 10.1371/journal.pone.0157454. eCollection 2016.
45. Brugat, T., et al., *Sequestration and histopathology in Plasmodium chabaudi malaria are influenced by the immune response in an organ-specific manner.* Cell Microbiol, 2014. **16**(5): p. 687-700.
46. Deroost, K., et al., *Hemozoin induces hepatic inflammation in mice and is differentially associated with liver pathology depending on the Plasmodium strain.* PLoS One, 2014. **9**(11): p. e113519.
47. Garcia-Romo, G.S., et al., *Netting neutrophils are major inducers of type I IFN production in pediatric systemic lupus erythematosus.* Sci Transl Med, 2011. **3**(73): p. 73ra20.
48. Marsman, G., S. Zeerleder, and B.M. Luken, *Extracellular histones, cell-free DNA, or nucleosomes: differences in immunostimulation.* Cell Death Dis, 2016. **7**(12): p. e2518.
49. Maina, R.N., et al., *Impact of Plasmodium falciparum infection on haematological parameters in children living in Western Kenya.* Malar J, 2010. **9 Suppl 3**: p. S4.
50. Olliaro, P., et al., *Hematologic parameters in pediatric uncomplicated Plasmodium falciparum malaria in sub-Saharan Africa.* Am J Trop Med Hyg, 2011. **85**(4): p. 619-25.
51. Kotepui, M., et al., *Effects of malaria parasite density on blood cell parameters.* PLoS One, 2015. **10**(3): p. e0121057.
52. Soehnlein, O., et al., *Neutrophils as protagonists and targets in chronic inflammation.* Nat Rev Immunol, 2017. **17**(4): p. 248-261.
53. Yang, L., et al., *ICAM-1 regulates neutrophil adhesion and transcellular migration of TNF-alpha-activated vascular endothelium under flow.* Blood, 2005. **106**(2): p. 584-92.
54. Cunningham, D.A., et al., *ICAM-1 is a key receptor mediating cytoadherence and pathology in the Plasmodium chabaudi malaria model.* Malar J, 2017. **16**(1): p. 185.
55. Smith, J.D., et al., *Identification of a Plasmodium falciparum intercellular adhesion molecule-1 binding domain: a parasite adhesion trait implicated in cerebral malaria.* Proc Natl Acad Sci U S A, 2000. **97**(4): p. 1766-71.
56. Cabrera, A., D. Neculai, and K.C. Kain, *CD36 and malaria: friends or foes? A decade of data provides some answers.* Trends Parasitol, 2014. **30**(9): p. 436-44.
57. Stoiser, B., et al., *Serum concentrations of granulocyte-colony stimulating factor in complicated Plasmodium falciparum malaria.* Eur Cytokine Netw, 2000. **11**(1): p. 75-80.
58. Aitken, E.H., A. Alemu, and S.J. Rogerson, *Neutrophils and Malaria.* Front Immunol, 2018. **9**: p. 3005.
59. Graca-Souza, A.V., et al., *Neutrophil activation by heme: implications for inflammatory processes.* Blood, 2002. **99**(11): p. 4160-5.

60. Dutra, F.F. and M.T. Bozza, *Heme on innate immunity and inflammation.* Frontiers in Pharmacology, 2014. **5**(115).
61. Rodrigues-da-Silva, R.N., et al., *Alterations in cytokines and haematological parameters during the acute and convalescent phases of Plasmodium falciparum and Plasmodium vivax infections.* Mem Inst Oswaldo Cruz, 2014. **109**(2): p. 154-62.
62. Ladhani, S., et al., *Changes in white blood cells and platelets in children with falciparum malaria: relationship to disease outcome.* Br J Haematol, 2002. **119**(3): p. 839-47.
63. Tobon-Castano, A., E. Mesa-Echeverry, and A.F. Miranda-Arboleda, *Leukogram Profile and Clinical Status in vivax and falciparum Malaria Patients from Colombia.* J Trop Med, 2015. **2015**: p. 796182.
64. Squire, D.S., et al., *Effect of Plasmodium falciparum malaria parasites on haematological parameters in Ghanaian children.* J Parasit Dis, 2016. **40**(2): p. 303-11.
65. Turner, G.D., et al., *An immunohistochemical study of the pathology of fatal malaria. Evidence for widespread endothelial activation and a potential role for intercellular adhesion molecule-1 in cerebral sequestration.* Am J Pathol, 1994. **145**(5): p. 1057-69.
66. Tessema, S.K., et al., *Antibodies to Intercellular Adhesion Molecule 1-Binding Plasmodium falciparum Erythrocyte Membrane Protein 1-DBLbeta Are Biomarkers of Protective Immunity to Malaria in a Cohort of Young Children from Papua New Guinea.* Infect Immun, 2018. **86**(8).
67. Oleinikov, A.V., et al., *A plasma survey using 38 PfEMP1 domains reveals frequent recognition of the Plasmodium falciparum antigen VAR2CSA among young Tanzanian children.* PLoS One, 2012. **7**(1): p. e31011.
68. Taylor, W.R.J., et al., *Respiratory manifestations of malaria.* Chest, 2012. **142**(2): p. 492-505.
69. Kolaczkowska, E., et al., *Molecular mechanisms of NET formation and degradation revealed by intravital imaging in the liver vasculature.* Nat Commun, 2015. **6**: p. 6673.
70. Tanaka, K., et al., *In vivo characterization of neutrophil extracellular traps in various organs of a murine sepsis model.* PLoS One, 2014. **9**(11): p. e111888.
71. Meng, W., et al., *Depletion of neutrophil extracellular traps in vivo results in hypersusceptibility to polymicrobial sepsis in mice.* Crit Care, 2012. **16**(4): p. R137.
72. Jimenez-Alcazar, M., et al., *Host DNases prevent vascular occlusion by neutrophil extracellular traps.* Science, 2017. **358**(6367): p. 1202-1206.
73. Fuchs, T.A., et al., *Extracellular DNA traps promote thrombosis.* Proc Natl Acad Sci U S A, 2010. **107**(36): p. 15880-5.
74. Albrengues, J., et al., *Neutrophil extracellular traps produced during inflammation awaken dormant cancer cells in mice.* Science, 2018. **361**(6409).
75. Yang, Z. Han, and J.J. Oppenheim, *Alarmins and immunity.* Immunol Rev, 2017. **280**(1): p. 41-56.
76. Lim, C.H., et al., *Thrombin and Plasmin Alter the Proteome of Neutrophil Extracellular Traps.* Front Immunol, 2018. **9**: p. 1554.
77. O'Sullivan, J.M., et al., *Emerging roles for hemostatic dysfunction in malaria pathogenesis.* Blood, 2016. **127**(19): p. 2281-8.
78. Ferreira, A., et al., *Sickle hemoglobin confers tolerance to Plasmodium infection.* Cell, 2011. **145**(3): p. 398-409.
79. Thobakgale, C.F. and T. Ndung'u, *Neutrophil counts in persons of African origin.* Curr Opin Hematol, 2014. **21**(1): p. 50-7.

80. Reiner, A.P., et al., *Genome-wide association study of white blood cell count in 16,388 African Americans: the continental origins and genetic epidemiology network (COGENT).* PLoS Genet, 2011. **7**(6): p. e1002108.
81. Elphinstone, R.E., et al., *Alterations in Systemic Extracellular Heme and Hemopexin Are Associated With Adverse Clinical Outcomes in Ugandan Children With Severe Malaria.* J Infect Dis, 2016. **214**(8): p. 1268-75.
82. Ramos, S., et al., *Renal control of disease tolerance to malaria.* Proc Natl Acad Sci U S A, 2019. **116**(12): p. 5681-5686.
83. *Berg A, Patel S, Aukrust P, David C, Gonca M, Berg ES, et al. Increased severity and mortality in adults co-infected with malaria and HIV in Maputo, Mozambique: a prospective cross-sectional study. PLoS One 2014;9(2):e88257. PMID: 24505451*.
84. de Chaumont, F., et al., *Icy: an open bioimage informatics platform for extended reproducible research.* Nat Methods, 2012. **9**(7): p. 690-6.
85. Harbort, C.J., et al., *Neutrophil oxidative burst activates ATM to regulate cytokine production and apoptosis.* Blood., 2015. **126**(26): p. 2842-51. doi: 10.1182/blood-2015-05-645424. Epub 2015 Oct 21.
86. Young, R.E., et al., *Neutrophil elastase (NE)-deficient mice demonstrate a nonredundant role for NE in neutrophil migration, generation of proinflammatory mediators, and phagocytosis in response to zymosan particles in vivo.* J Immunol, 2004. **172**(7): p. 4493-502.
87. Warnatsch, A., et al., *Inflammation. Neutrophil extracellular traps license macrophages for cytokine production in atherosclerosis.* Science, 2015. **349**(6245): p. 316-20.
88. Kenny, E.F., et al., *Dnase1-deficient mice spontaneously develop a systemic lupus erythematosus-like disease.* Eur J Immunol, 2019.
89. Li, P., et al., *PAD4 is essential for antibacterial innate immunity mediated by neutrophil extracellular traps.* J Exp Med, 2010. **207**(9): p. 1853-62.
90. Swamydas, M., et al., *Isolation of Mouse Neutrophils.* Curr Protoc Immunol, 2015. **110**: p. 3 20 1-3 20 15.
91. Brinkmann, V., et al., *Automatic quantification of in vitro NET formation.* Front Immunol, 2012. **3**: p. 413.
92. Losman, M.J., et al., *Monoclonal autoantibodies to subnucleosomes from a MRL/Mp(-)+/+ mouse. Oligoclonality of the antibody response and recognition of a determinant composed of histones H2A, H2B, and DNA.* J Immunol, 1992. **148**(5): p. 1561-9.
93. Weis, S., et al., *Metabolic Adaptation Establishes Disease Tolerance to Sepsis.* Cell, 2017. **169**(7): p. 1263-1275 e14.
94. Amulic, B., et al., *An upstream open reading frame controls translation of var2csa, a gene implicated in placental malaria.* PLoS Pathog, 2009. **5**(1): p. e1000256.
95. Barrera, V., et al., *Host fibrinogen stably bound to hemozoin rapidly activates monocytes via TLR-4 and CD11b/CD18-integrin: a new paradigm of hemozoin action.* Blood, 2011. **117**(21): p. 5674-82.
96. Viriyavejakul, P., V. Khachonsaksumet, and C. Punsawad, *Liver changes in severe Plasmodium falciparum malaria: histopathology, apoptosis and nuclear factor kappa B expression.* Malar J, 2014. **13**: p. 106.
97. Matute-Bello, G., et al., *An official American Thoracic Society workshop report: features and measurements of experimental acute lung injury in animals.* Am J Respir Cell Mol Biol, 2011. **44**(5): p. 725-38.

98. Virreira Winter, S. and A. Zychlinsky, *The bacterial pigment pyocyanin inhibits the NLRP3 inflammasome through intracellular reactive oxygen and nitrogen species.* J Biol Chem, 2018. **293**(13): p. 4893-4900.
99. Vancurova, I., V. Miskolci, and D. Davidson, *NF-kappa B activation in tumor necrosis factor alpha-stimulated neutrophils is mediated by protein kinase Cdelta. Correlation to nuclear Ikappa Balpha.* J Biol Chem, 2001. **276**(23): p. 19746-52.

**Acknowledgements:** We would like to thank the patients, physicians, nurses and other staff at the Albert-Schweitzer and at Maputo Central Hospitals for their support and aid during our study. We also thank Dr Karl Seydel and Prof Terrie Taylor for access to histopathology samples.

BA is an MRC Career Development Fellow. AC is supported by MRC and the UK Department for International Development (DFID) under the MRC/DFID Concordat agreement and is also part of the EDCTP2 program supported by the European Union (MR/L006529/1 to AC). AG was supported by an Imperial College Dean's Internship Award.

**Author contributions:** BA, SLK, AZ, AC, CM and BR conceived and designed the experiments. LK, BA, FA, AG performed the experiments. UAA, VB and AG performed microscopy. AB, RK, VB, SH, SP, KO, BM and CM contributed clinical samples. DC, JL, ES contributed with reagents/materials. BA, LK and AZ wrote/drafted and finalized the paper. All authors read and approved the final manuscript.

**Competing interests:** The authors report no competing interests.

1072 **Figure 1**

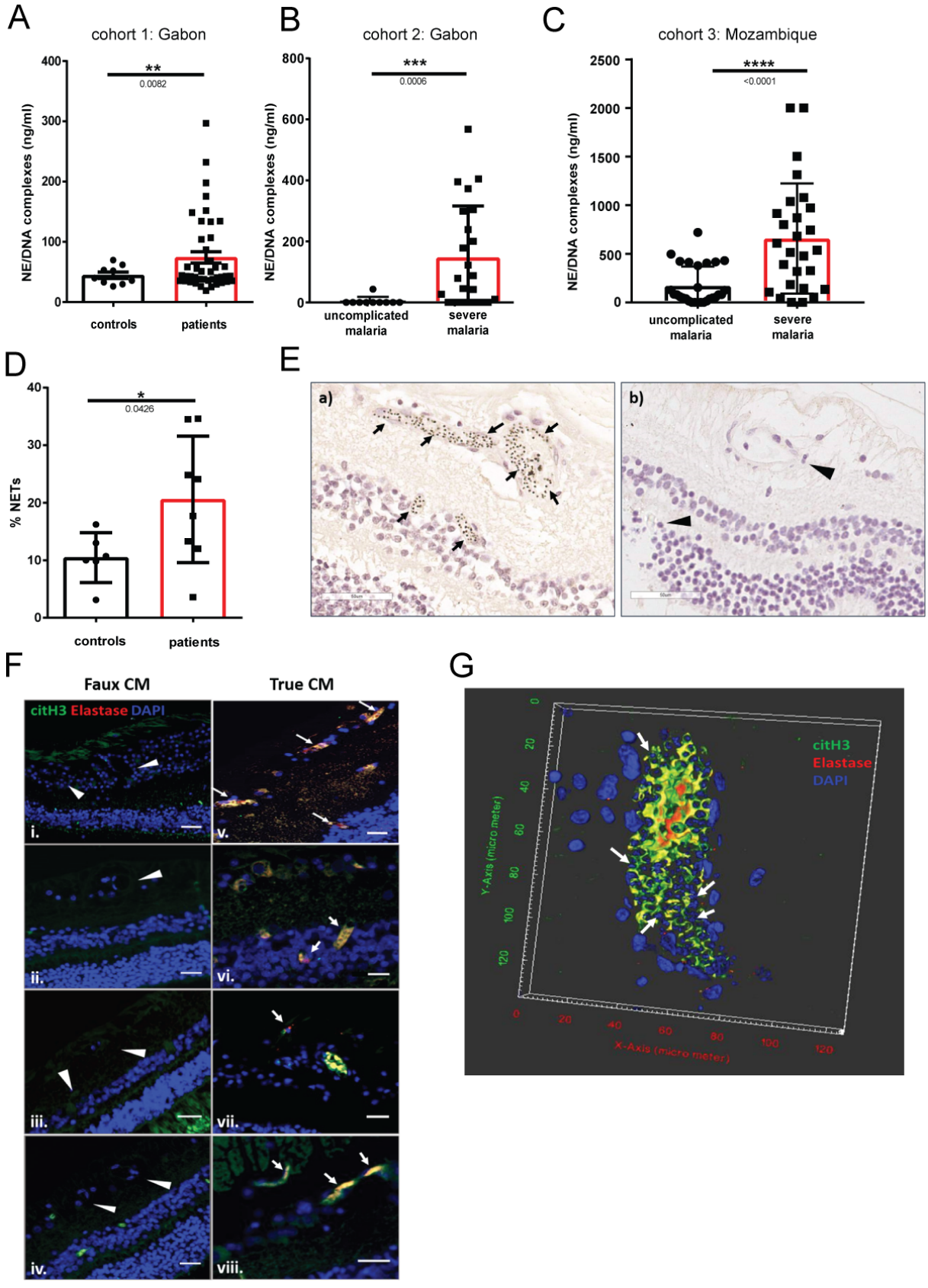


1073

**Figure 1: *P. falciparum* infection induces accumulation of NETs in circulation**

Circulating NET components (NE/DNA complexes) measured by ELISA in plasma from patients in three different malaria cohorts: (**A**) mixed age uncomplicated malaria (n=43) and healthy controls in Gabon (n=9), (**B**) pediatric uncomplicated (n=10) and severe malaria (n=23) patients in Gabon and (**C**) adult uncomplicated (n=28) and severe malaria (n=27) patients in Mozambique. **(D)** Quantification of NETosis in neutrophils isolated from healthy individuals and malaria patients. **(E)** H&E images of a) retinopathy positive CM cases showing extensive sequestration (arrows) of parasites on the retinal endothelium. Mature parasites appear as black dots due to hemozoin pigment accumulated in their food vacuole. b) Retinopathy negative CM case showing no sequestration in the vasculature (arrowheads point to the capillaries). Scale bar = 50μm. **(F)** Merged images stained with citrullinated histone H3 (green), elastase (red) and DAPI (blue). Arrows indicate NETs, visualized by co-localization of all the stained components. Arrowheads point to the capillaries of retinopathy negative cases which show no sequestration. Scale bar = 25 μm. Figure shows representative images from 9 different 'true' CM and 8 different 'faux' CM cases. **(G)** 3D reconstruction of capillary with very high sequestration, by z-stack images collected from a true CM case. Merged image with citrullinated histone H3 (green), elastase (red), and DAPI (blue). DAPI stains the parasite DNA inside the parasitized erythrocytes (arrows) as well as the nuclei of the host cells. Data is presented as the mean ± standard error of the mean (SEM). Asterisks indicate significance: *P<.05, **P<.01, ***P<.001 by Welch's t-test.

1101 Figure 2

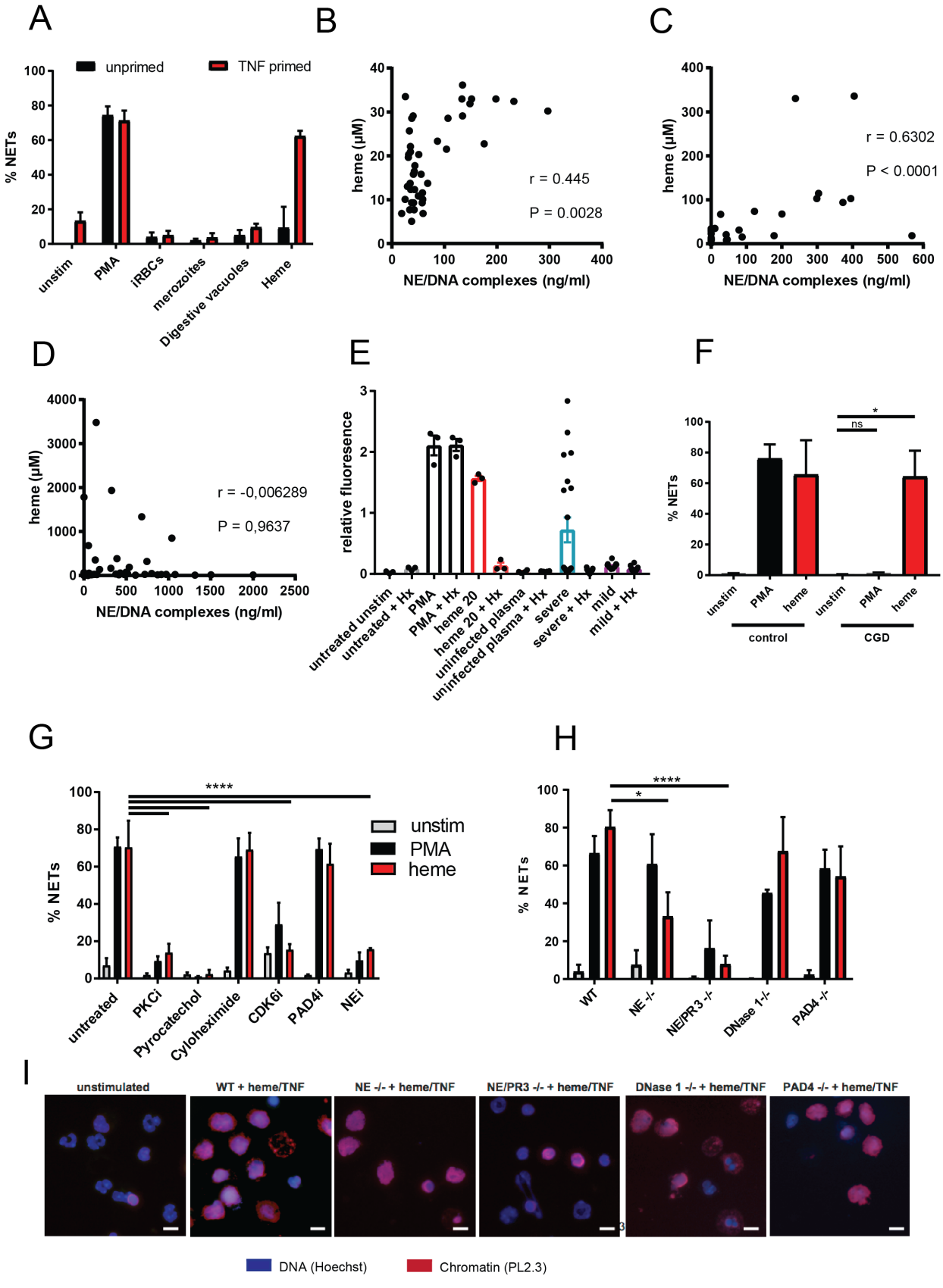


1102

**Figure 2: Heme induces NETs in a mechanism requiring serine proteases**

**(A)** *In vitro* stimulation of neutrophils isolated from healthy individuals (n=3) with malaria associated PAMPs and DAMPs (n = 3). **(B - D)** Spearman correlation of NETs and heme concentration in malaria patients of all three cohorts presented in Fig. 1. **(E)** Quantification of NETosis of healthy neutrophils in response to plasma (10% v/v) from malaria patients, PMA (50 nM) or heme (20 μM) in combination with TNF priming. Hx refers to treatment with 70 μM hemopexin for 30 min prior to stimulation. **(F)** Quantification of NETosis in neutrophils from healthy donors (n=3) and CGD patients (n=3) in response to PMA and heme. **(G)** Quantification of NETosis in response to PMA and heme in neutrophils from healthy donors (n=3) preincubated with inhibitors at the following concentrations: 1 μM Go6983 (PKCi), 30 uM pyrochatecol, 1 μg/ml cycloheximide, 2.5 μM abemaciclib (CDK6i), 10 μM BB-Cl-amideine (PAD4i) and 20 μM GW311616A (NEi) . **(H)** Quantification of NET formation in mouse peritoneal neutrophils (n = 3) in response to PMA (100 nM) and heme (20 μM) with TNF pretreatment. (**F-H**): all graphs display mean ± SEM. **(I)** Representative images used for mouse NET quantifications, showing staining for DNA (blue) and histone H2A/H2B-DNA (red). Scale bars = 20 μm. Asterisks indicate significance: *P<.05, **P<.01, ***P<.001 by Welch's t-test.

Figure 3

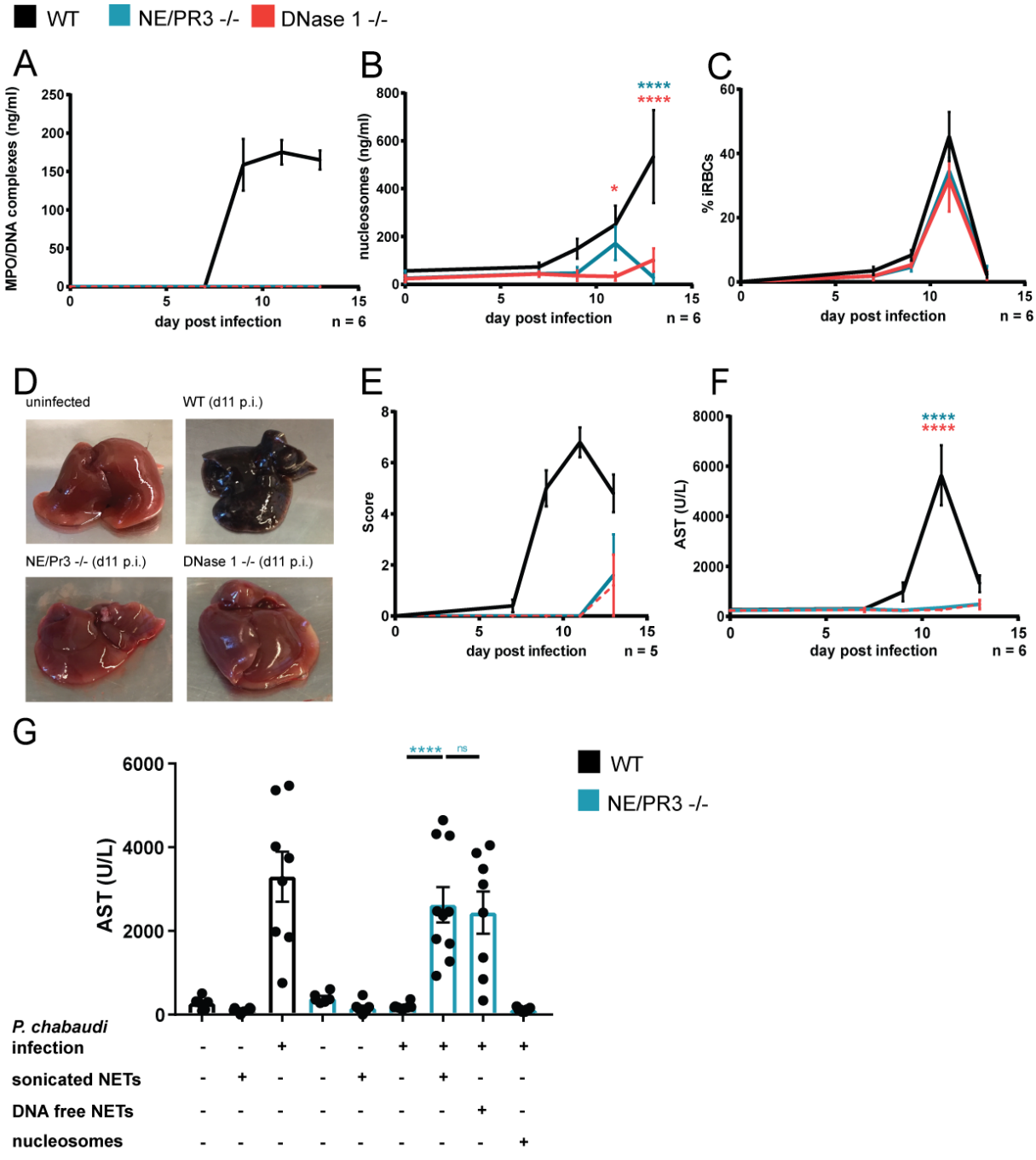
WT
NE/PR3 -/-
DNase 1 -/-
A
MPO/DNA complexes (ng/ml)
day post infection
n = 6
B
nucleosomes (ng/ml)
****
****
*
day post infection
n = 6
C
% iRBCs
day post infection
n = 6
D
uninfected
WT (d11 p.i.)
NE/Pr3 -/- (d11 p.i.)
DNase 1 -/- (d11 p.i.)
E
Score
day post infection
n = 5
F
AST (U/L)
****
****
day post infection
n = 6
G
AST (U/L)
****
ns
WT
NE/PR3 -/-
P. chabaudi infection
sonicated NETs
DNA free NETs
nucleosomes

**Figure 3: Extracellular NET components are associated with disease severity.**

ELISA quantifications of **(A)** NETs (MPO/DNA complexes) and **(B)** extracellular nucleosomes, in plasma over the course of a *P. chabaudi* infection. **(C)** Parasitemia from Giemsa stained blood smears. **(D)** Representative livers of experimental animals showing severe discoloration in infected WT animals. **(E)** Blinded pathology scores of livers and **(F)** concentration of aspartate aminotransferase (AST) in plasma. n = 5-6 (indicated under the graphs). Data is presented as mean ± SEM. Asterisks indicate significance: *P<.05, **P<.01, ***P<.001 and ****P<0.0001 by two-way analysis of variance (ANOVA) comparison of 3 groups. Color of the asterisks indicate which genotype they refer to. **(G)** AST in plasma of experimental animals treated as indicated, at peak parasitemia. n = 6-10. Data is presented as mean ± SEM. Asterisks indicate significance: *P<.05, **P<.01, ***P<.001 and ****P<0.0001 by Mann-Whitney test.

1140 Figure 4

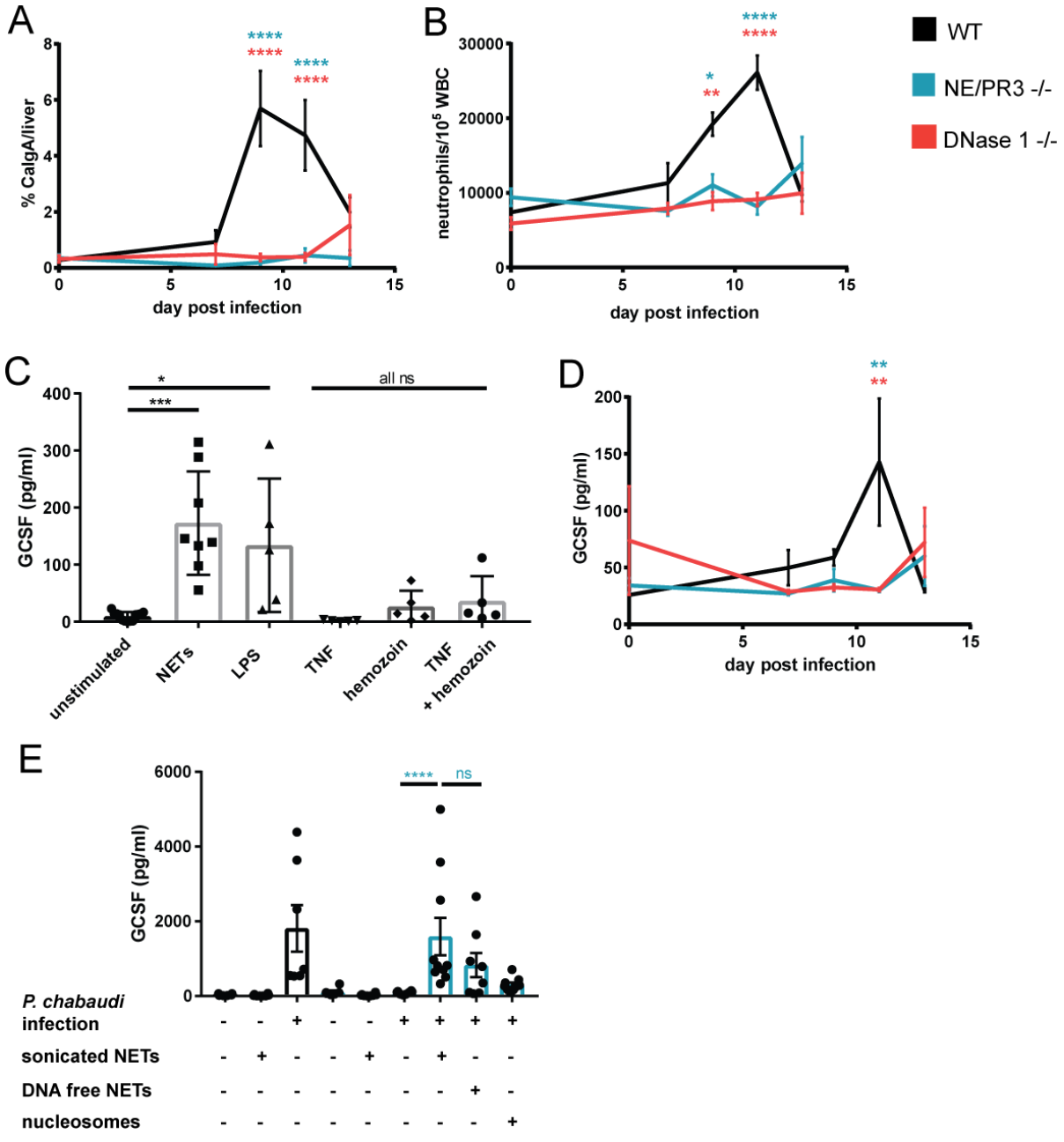


1141

1142

1143

1144

1145

**Figure 4: NET components induce emergency granulopoiesis and GCSF production.**

**(A)** Microscopic quantification of neutrophil liver infiltrates using immunofluorescence for calgranulin A. Data is presented as calgranulin A signal (neutrophils) normalized to DAPI (total liver area). **(B)** Ratio of neutrophils to leukocytes determined by FACS analysis of whole blood samples. Neutrophils were defined as CD45+, CD3-, Ly6G/C high, CD115-. **(C)** GCSF in supernatants of human macrophages (n=5) stimulated for 12 h with NETs (1 µg/ml), LPS (500 ng/ml), TNF (2 ng/ml) and/or hemozoin (100 µg/ml). **(D)** Plasma GCSF concentration. n = 6 for all *in vivo* data. Data is presented as mean ± SEM. Asterisks indicate significance: A,B and D: *P<.05, **P<.01, ***P<.001 and ****P<0.0001 by two-way analysis of variance (ANOVA) comparison of 3 groups. Color of the asterisks indicate which genotype they refer to. **(E)** Plasma GCSF concentration at peak parasitemia in experimental animals receiving indicated treatments. n = 6-10 (indicated by number of dots). Data is presented as mean ± SEM. Asterisks indicate significance: *P<.05, **P<.01, ***P<.001 and ****P<0.0001 by Mann-Whitney test.

Figure 5

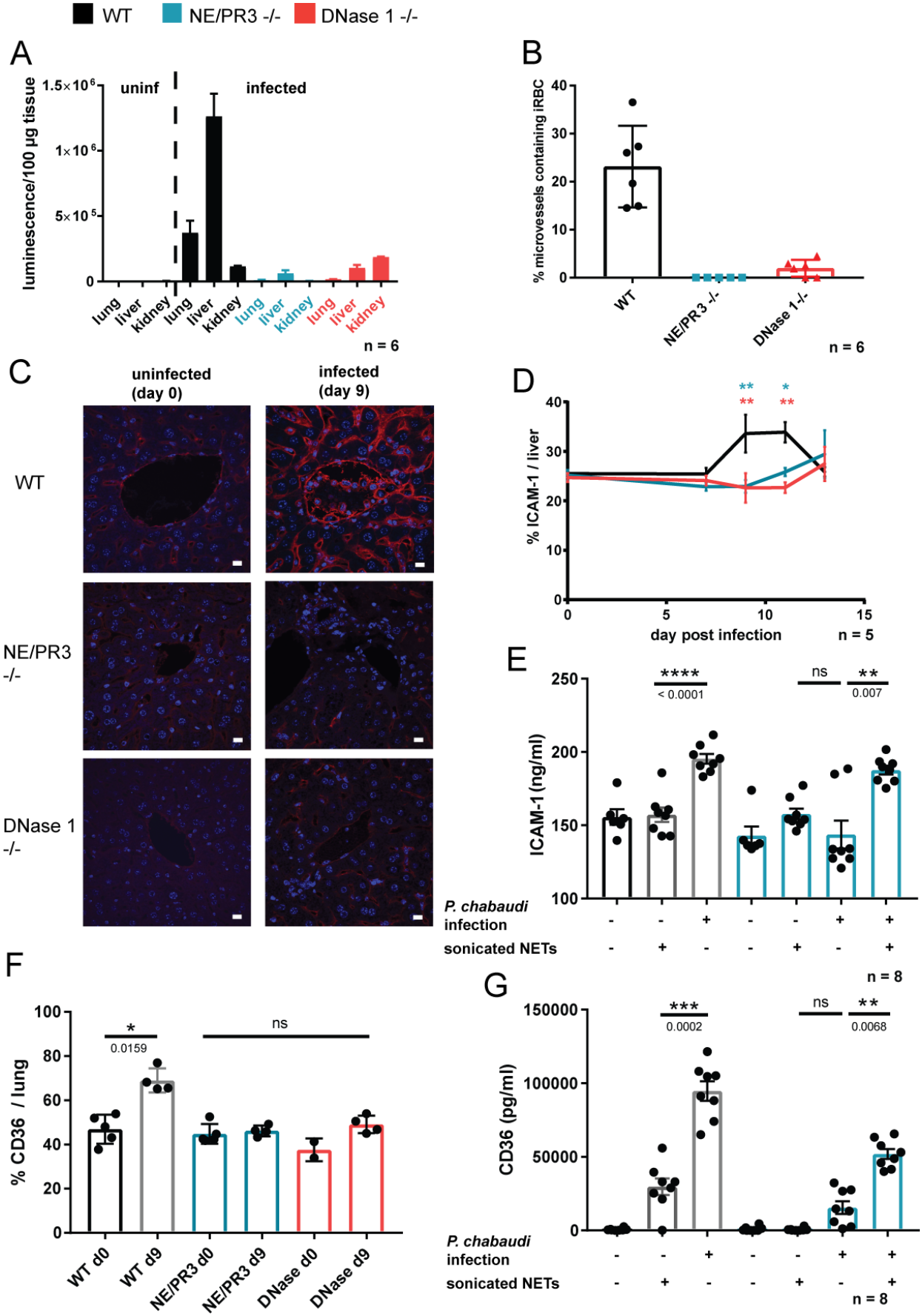
WT
NE/PR3 -/-
DNase 1 -/-
A
luminescence/100 µg tissue
1.5×10⁶
1×10⁶
5×10⁵
0
uninf
infected
lung
liver
kidney
n = 6
B
% microvessels containing iRBC
40
30
20
10
0
WT
NE/PR3 -/-
DNase 1-/-
n = 6
C
uninfected (day 0)
infected (day 9)
WT
NE/PR3 -/-
DNase 1 -/-
D
% ICAM-1 / liver
**
**
*
**
day post infection
n = 5
E
ICAM-1 (ng/ml)
250
200
150
100
****
< 0.0001
ns
**
0.007
P. chabaudi infection
sonicated NETs
n = 8
F
% CD36 / lung
100
80
60
40
20
0
*
0.0159
ns
WT d0
WT d9
NE/PR3 d0
NE/PR3 d9
DNase d0
DNase d9
G
CD36 (pg/ml)
150000
100000
50000
0
***
0.0002
ns
**
0.0068
P. chabaudi infection
sonicated NETs
n = 8

**Figure 5: NETs promote parasite sequestration and endothelial activation.**

**(A)** Parasite sequestration in different organs measured by quantification of luminescence from a luciferase expressing strain of *P. chabaudi*; n=6 mice. **(B)** Histological quantification of parasites sequestered in the microvasculature of the liver from H&E images; n=6. **(C)** Representative images of immunofluorescence staining of ICAM-1 (red) and DNA (blue) in the livers of experimental animals. **(D)** Quantification of ICAM-1 signal from (**C**), normalized to DAPI (total liver area); n=6. **(E)** Soluble ICAM-1 in plasma of experimental animals treated as indicated; n=8. **(F)** Immunofluorescence microscopy quantification of CD36 expression in lung sections, normalised to DAPI signal (total lung area); n=2-5 (indicated by number of dots). **(G)** CD36 concentration in plasma measured by ELISA (n=8). Data is presented as mean ± SEM. Asterisks indicate significance. D: *P<.05, **P<.01, ***P<.001 and ****P<0.0001 by two-way analysis of variance (ANOVA) comparison of 3 groups. Color of the asterisks indicate which genotype they refer to. E-G: *P<.05, **P<.01, ***P<.001 and ****P<0.0001 by Mann-Whitney test.

Figure 6

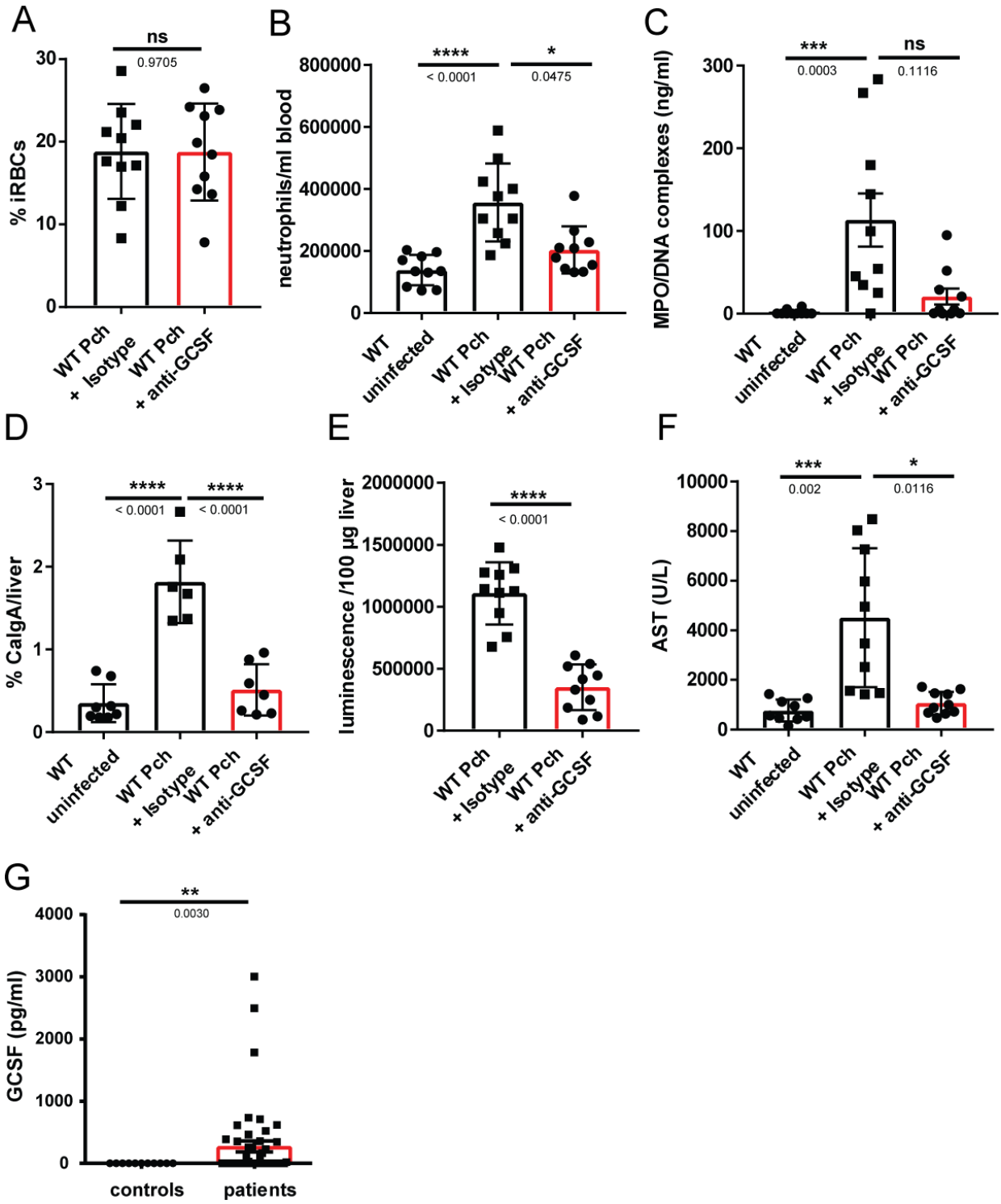
A
ns
0.9705
% iRBCs
30
20
10
0
WT Pch + Isotype
WT Pch + anti-GCSF
B
****
< 0.0001
*
0.0475
neutrophils/ml blood
800000
600000
400000
200000
0
WT uninfected
WT Pch + Isotype
WT Pch + anti-GCSF
C
***
0.0003
ns
0.1116
MPO/DNA complexes (ng/ml)
300
200
100
0
WT uninfected
WT Pch + Isotype
WT Pch + anti-GCSF
D
****
< 0.0001
****
< 0.0001
% CalgA/liver
3
2
1
0
WT uninfected
WT Pch + Isotype
WT Pch + anti-GCSF
E
****
< 0.0001
luminescence /100 µg liver
2000000
1500000
1000000
500000
0
WT Pch + Isotype
WT Pch + anti-GCSF
F
***
0.002
*
0.0116
AST (U/L)
10000
8000
6000
4000
2000
0
WT uninfected
WT Pch + Isotype
WT Pch + anti-GCSF
G
**
0.0030
GCSF (pg/ml)
4000
3000
2000
1000
0
controls
patients

**Figure 6: GCSF neutralisation is protective in malaria.**

**(A)** Parasitemia of infected mice (n=10) measured by counting thin blood smears. **(B)** Absolute counts of circulating neutrophils determined by FACS. Neutrophils were labelled with an anti-Ly6G antibody (n=10). **(C)** NETs (MPO/DNA complexes) in plasma quantified by ELISA (n=10). **(D)** Neutrophil liver infiltrates quantified by analysis of calgranulin A immunofluorescence in liver sections (n=6). **(E)** Parasite sequestration in the liver (n=10), measured by luminescence quantification of a luciferase expressing strain of *P. chabaudi.* **(F)** Concentration of AST in plasma of mice at peak parasitemia (n = 10). Data is presented as mean ± SEM, each dot represents one biological replicate. Asterisks indicate significance: *P<.05, **P<.01, ***P<.001 and ****P<0.0001 by Kruskall-Wallis test **(G)** GCSF concentration in plasma of uncomplicated malaria patients (n=43) and healthy individuals (n=9) in Gabon. Data is presented as the mean ± SEM. Asterisks indicate significance: *P<.05, **P<.01, ***P<.001 by Welch's t-test.

**Figure S1**

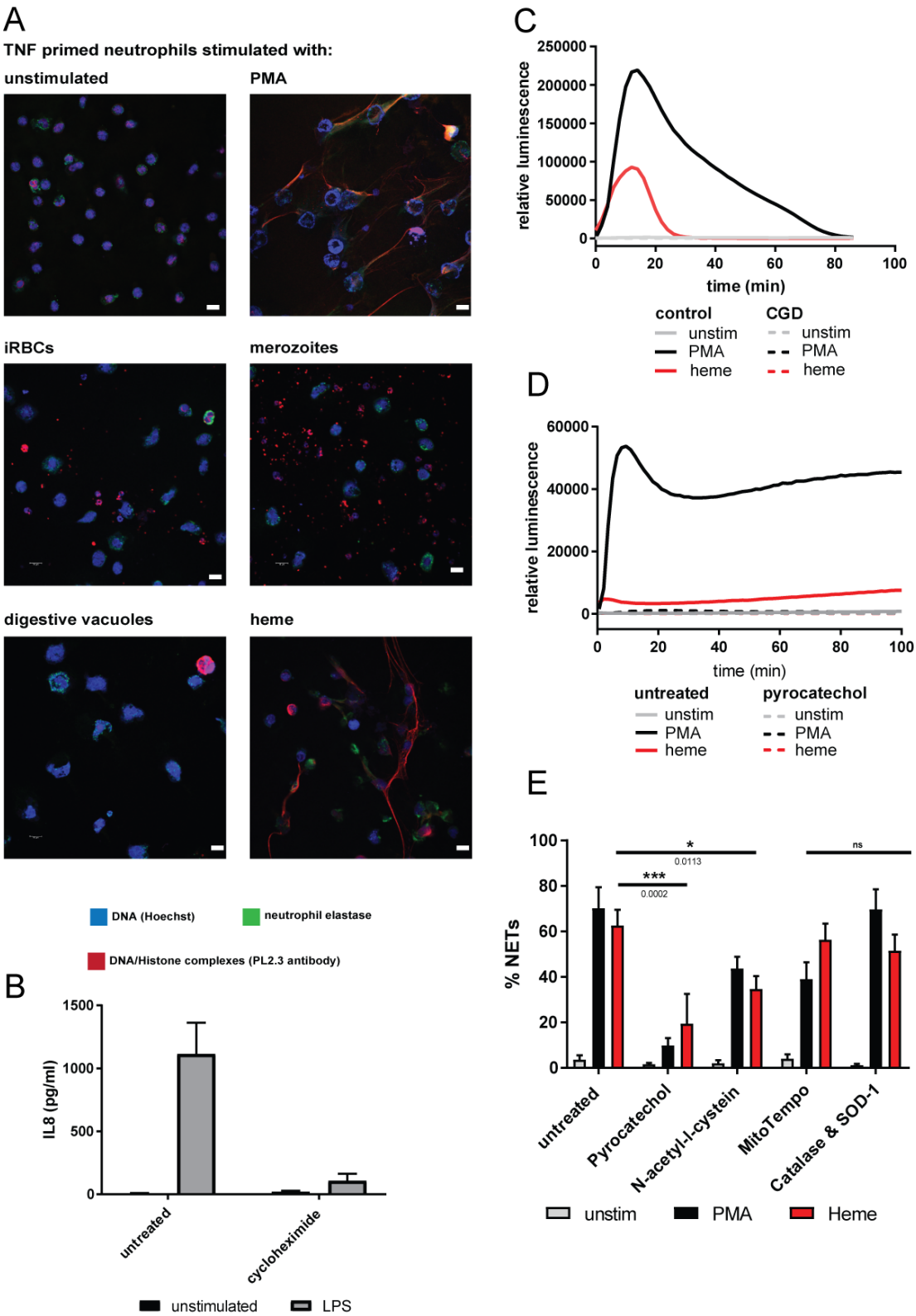


**Supplementary Figure 1: In vitro stimulations of human neutrophils**

**(A)** Confocal microscopy images of TNF primed neutrophils stimulated with malaria associated PAMPs and DAMPs; PMA serves as a positive control. Scale bars represent 20 µm. **(B)** IL-8 ELISA of supernatants from neutrophils treated with LPS. IL-8 is not stored in the neutrophil and its release requires translation. **(C)** Production of ROS measured by luminol assay **(D)** Production of ROS by neutrophils treated with pyrocatechol. Cells are unable to produce ROS in response to both PMA or heme.**(E)** Quantification of NET formation induced by PMA or heme in healthy human neutrophils pretreated with the indicated ROS scavenging agents at the following concentrations: 30 µM Pyrochatecol, 10 mM N-acetyl-l-cysteine. 10 µM MitoTempo, 10 ng/µl Catalase & 10 ng/µl SOD-1. Data is presented as the mean ± SEM.

1234

## Figure S2:

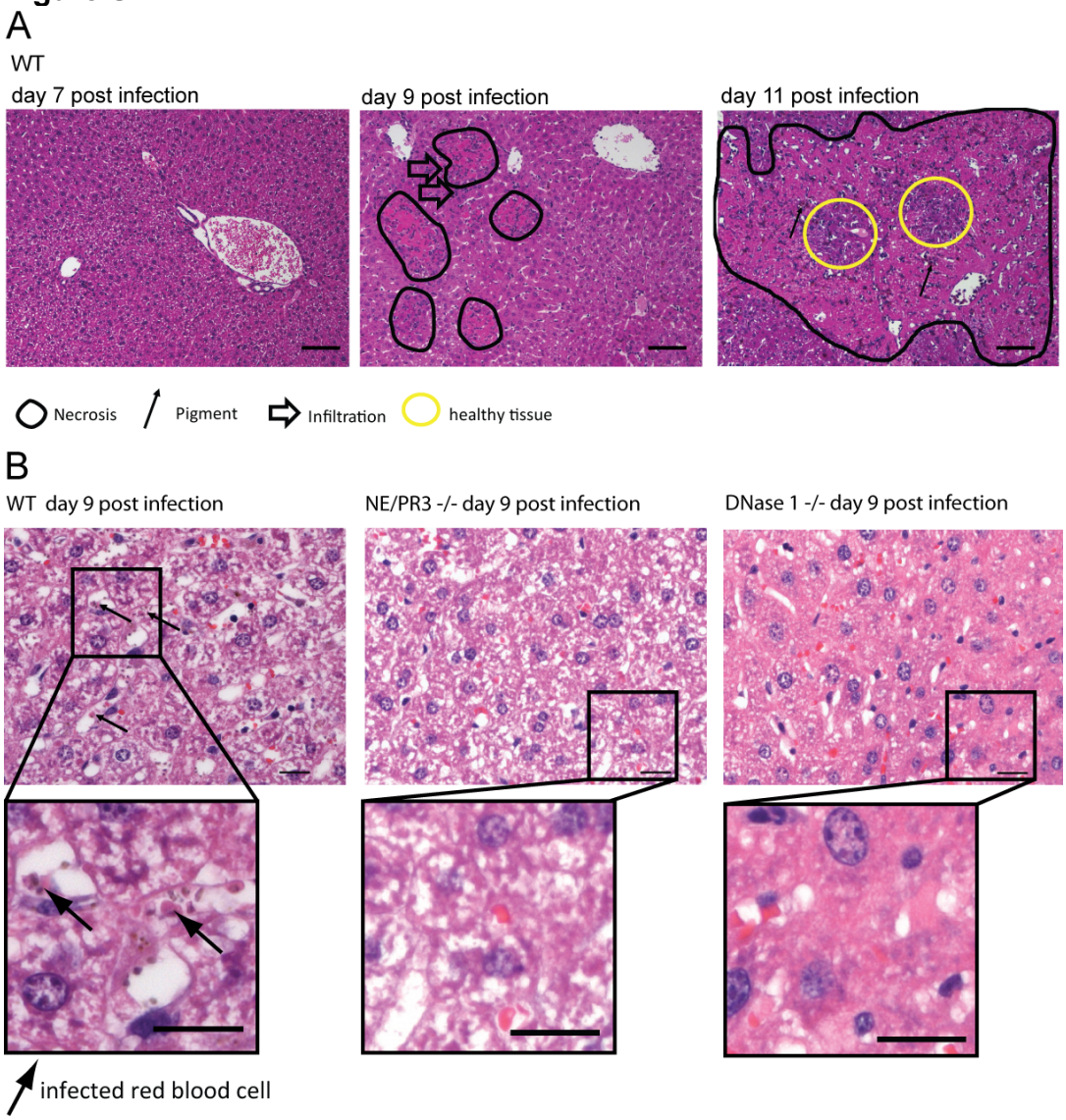


**Supplementary Figure 2: Necrosis and sequestration in the livers of *P. chabaudi* infected mice.** **(A)** Sample images of H&E stained liver sections used to quantify liver damage. Black outlines indicate areas containing necrotic liver cells, large arrows indicate immune cell infiltration and yellow outlines indicated healthy tissue surrounded by necrosis. Analysis was performed blinded by a pathologist, scale bar equals 100 μm. **(B)** Representative H&E stained images of livers from infected animals, arrows indicate iRBCs bound to the endothelium, scale bar equals 20 μm. **(C)** Electron micrograph of an infected red blood cell attached to the vasculature in the liver of a WT mice.

## Figure S3

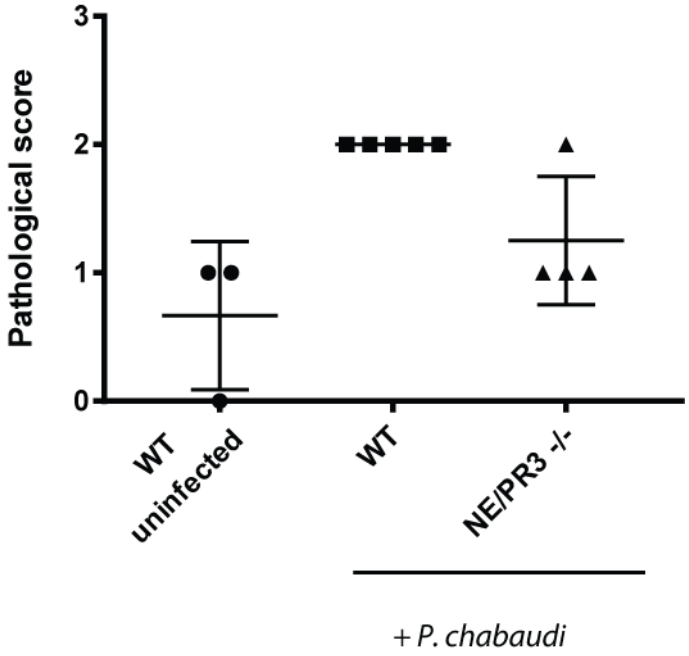


**Figure S3: Pathology in the lungs of *P. chabaudi* infected animals.** Blinded scoring of lungs from infected animals at peak parasitemia, according to score sheet presented in Methods.

**Figure S4:**

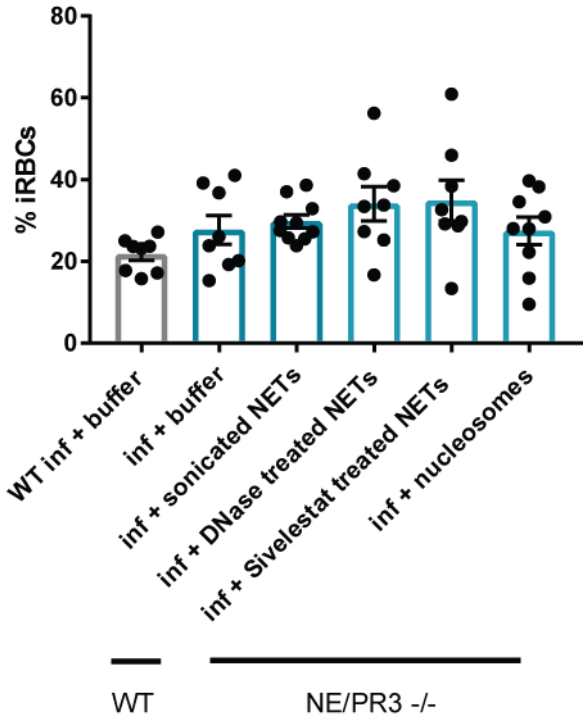


**Figure S4: Parasitemia of NET fragment injected mice.** Parasitemia of infected animals quantified by counting Giemsa stained thin blood smears.

**Figure S5:**

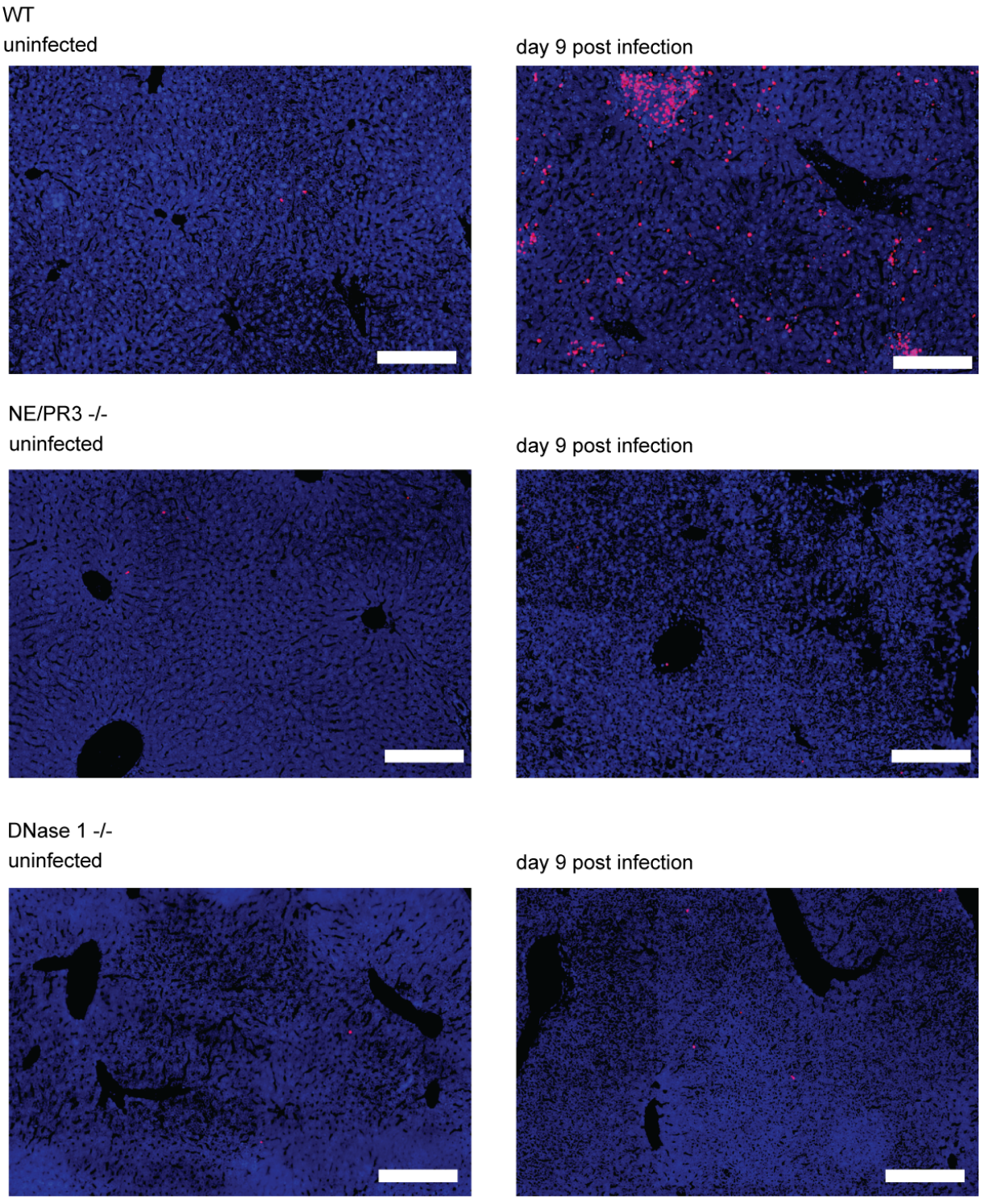


**Figure S5: Immunofluorescence images used to quantify neutrophils in livers of infected mice.** Sample images of livers from infected animals of indicated genotypes stained with Hoechst (blue) and a neutrophil specific anti-Calgranulin A antibody (red).

## Figure S6

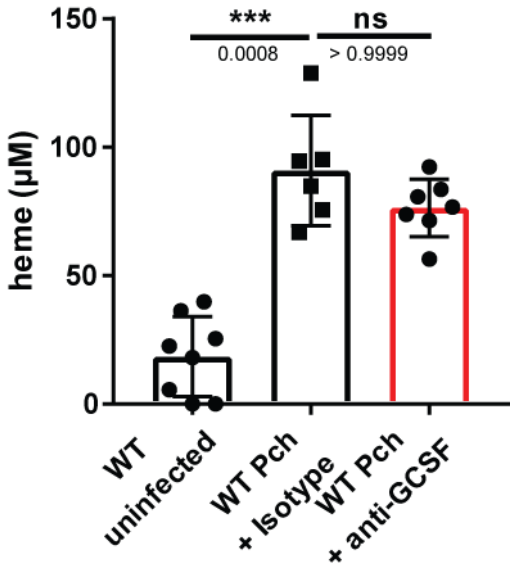


**Figure S6:** Quantification of free circulating heme in plasma of uninfected and infected animals, treated with a GCSF neutralizing antibody or isotype control antibody.

**Table S1: Patient information of cohort 1 & 2 in Gabon.**

| | Cohort 1 | Cohort 2 | |
|---|---|---|---|
| | uncomplicated | uncomplicated | severe |
| n | 43 | 10 | 23 |
| | Mean (min - max) | | |
| Age (years) | 1 (1 - 84) | 4 (3 - 7) | 4 (1 - 10) |
| Parasitemia (pf/µl) | 1635 (59 - 260113) | 7595 (2100 - 20000) | 335743 (2600 - 1100000 |
| Temperature (°C) | 38 (37 - 40) | n.a. | n.a. |
| Hematocrit (%) | 33.45 (19.2 - 44.9) | n.a. | n.a. |
| Hemoglobin (g/dl) | 10.1 (4.2 - 17.7) | 10.1 (9.1 - 12.2) | 8.76 (5 - 13.2) |

**Table S2: Clinical characteristics of the patient population in Mozambique.**

| | Uncomplicated malaria | | Severe malaria | |
|---|---|---|---|---|
| n | 28 | | 27 | |
| | Mean (min-max) | % proportion | Mean (min – max) | % proportion |
| Age | 36 (18-73) | | 42 (20-65) | |
| Sex (females) | | 35.7 (10/28) | | 44.4 (12/27) |
| Hb | 11.7 (5.9-15.7) | | 10.8 (3.2-17.0) | |
| WBC | 6.1 (2.2-12.4) | | 7.5 (1.3-15.5) | |
| Platelets | 119 (24-324) | | 127 (11-452) | |
| Creatinine | 108 (57-203) | | 152 (72-357) | |
| Se-glucosis | 9.0 (4.2-34.2) | | 9.0 (3.7-40.5) | |
| Systolic BP | 123 (90-240) | | 119 (70-160) | |
| Respiratory rate | 20 (14-28) | | 25 (16-68) | |
| Liver failure[a)] | | 0 | | 11.1 (3/27) |
| Coagulat. disturb.[b)] | | 0 | | 3.7 (1/27) |
| Cerebral disturb.[c)] | | 14.3 (4/28) | | 29.6 (8/27) |
| Case fatality rate | | 0[d)] | | 3.7 (1/27) |

[a)]Defined as jaundice and/or bilirubine>43µmol/L
[b)]Defined as bleeding disturbaces and/or hemolysis
[c)]Defined as Glascow Coma Scale≤11, repeated convulsions and/ or confusion
[d)] Two patients missing
Continuous variables given in mean (min-max), not rounded numbers.

**Table S3 Clinical diagnosis and classification of subjects whose ocular tissue was used for immunofluorescence experiments.**

| Sample | Before post-mortem clinical diagnosis | Post-mortem classification | Retinopathy |
|---|---|---|---|
| 1 | Clinical CM | 1 | Yes |
| 2 | Clinical CM | 1 | Yes |
| 3 | Clinical CM | 1 | Yes |
| 4 | Clinical CM | 1 | Yes |
| 5 | Clinical CM | 1 | Yes |
| 6 | Clinical CM + SMA | 2 | Yes |
| 7 | Clinical CM | 2 | Yes |
| 8 | Clinical CM, severe pneumonia, severe meningoencephalitis | 2 | Yes |
| 9 | Clinical CM | 2 | Yes |
| 10 | Clinical CM – pneumonia, Reye's syndrome | 3 | No |
| 11 | Clinical CM, likely cause of death is anaemia | 3 | No |
| 12 | Clinical CM + SMA, hepatitis | 3 | No |
| 13 | Clinical CM; Severe pneumonia | 3 | No |
| 14 | Clinical CM, severe pneumonia with spread to meninges | 3 | No |
| 15 | Clinical CM, left ventricular failure with pulmonary oedema | 3 | No |
| 16 | Clinical CM, fatal pneumonia | 3 | No |
| 17 | Salmonella sepsis | 7 | No |

Class 1 & 2 (CM1 & 2) are the “true CM” while Class 3 (CM3) are the “Faux CM”. CM3 mimics CM during life so these children are control for being really sick and for premorbid events but in fact there is no sequestration and there is an alternative cause of death – suggesting a different pathogenic process - so they represent an excellent comparator for sequestration driven pathology. Class 7= Non-malarial encephalopathy, infectious. SMA, severe malarial anaemia.